Role of astrocyte senescence regulated by the non-canonical autophagy in the neuroinflammation associated to cerebral malaria.

Fatima Hellani, Inès Leleu, Nasreddine Saidi, Nathalie Martin, Cecile Lecoeur, Elisabeth Werkmeister, D. Koffi, Francois Trottein, H. Yapo-Etté, B. Das, et al.

Brain, Behavior, and Immunity 117 (2024) 20–35

Contents lists available at ScienceDirect

Brain Behavior and Immunity

journal homepage: www.elsevier.com/locate/ybrbi

Full-length Article

Role of astrocyte senescence regulated by the non– canonical autophagy in the neuroinflammation associated to cerebral malaria

Fatima Hellani [a,1], Inès Leleu [a,1], Nasreddine Saidi [a,1], Nathalie Martin [b], Cécile Lecoeur [a], Elisabeth Werkmeister [c], David Koffi [d], François Trottein [a], Hélène Yapo-Etté [e], Bidyut Das [f], Corinne Abbadie [b], Sylviane Pied [a,*]

[a] Univ. Lille, CNRS UMR 9017-INSERM U1019, Center for Infection and Immunity of Lille-CIIL, Institut Pasteur de Lille F-59019 Lille, France
[b] Univ. Lille, CNRS, INSERM, CHU Lille, Institut Pasteur de Lille, UMR9020-U1277 - CANTHER - Cancer Heterogeneity, Plasticity and Resistance to Therapies F-59000 Lille, France
[c] Univ. Lille, CNRS, INSERM, CHU Lille, Institut Pasteur de Lille, US 41 - UMS 2014 - PLBS F-59000 Lille, France
[d] Parasitology and Mycology Department, Institut Pasteur de Côte d'Ivoire, Ivory Coast
[e] Institute of Forensic Medicine-Faculty of Health, University Félix Houphouët-Boigny of Abidjan, Ivory Coast
[f] SCB Medical College, Cuttack, Orissa, India

ARTICLE INFO

Keywords:
Astrocyte
Cellular senescence
P21
Cerebral malaria
Inflammation
Senolytic drugs

ABSTRACT

Background: Cerebral malaria (CM) is a fatal neuroinflammatory syndrome caused (in humans) by the protozoa *Plasmodium (P.) falciparum*. Glial cell activation is one of the mechanisms that contributes to neuroinflammation in CM.
Result: By studying a mouse model of CM (caused by *P. berghei* ANKA), we describe that the induction of autophagy promoted p21-dependent senescence in astrocytes and that CXCL-10 was part of the senescence-associated secretory phenotype. Furthermore, p21 expression was observed in post-mortem brain and peripheral blood samples from patients with CM. Lastly, we found that the depletion of senescent astrocytes with senolytic drugs abrogated inflammation and protected mice from CM.
Conclusion: Our data provide evidence for a novel mechanism through which astrocytes could be involved in the neuropathophysiology of CM. *p21* gene expression in blood cell and an elevated plasma CXCL-10 concentration could be valuable biomarkers of CM in humans. In the end, we believe senolytic drugs shall open up new avenues to develop newer treatment options.

1. Introduction

Cerebral malaria (CM) is the deadliest complication of a *Plasmodium (P.) falciparum* infection transmitted to humans by the bite of an infected female anopheles mosquito. According to the World Health Organization, malaria affects approximately 241 million people worldwide and resulted in 627,000 deaths from CM in 2020 (WHO, 2021). Young children and non-immune individuals (including pregnant women) are particularly affected in sub-Saharan Africa (WHO, 2021). Ataxia, seizure and coma before death and low peripheral parasitaemia are common features of CM (Idro et al., 2005). In endemic areas, about 25 % of CM survivors develop neurological sequelae (e.g. cognitive impairments), long-term mental health disorders, and behavioural difficulties (Boivin et al., 2007; Carter et al., 2005). Even though huge research efforts have been focused on the pathophysiology of CM, many aspects of this complex disease are still not understood and thus require further investigation.

In the C57BL/6 mouse model of CM induced by *P. berghei* ANKA (*PbA*), experimental cerebral malaria (ECM) is characterized by low accumulation of parasite-infected red blood cells (iRBCs) in mice as well as in human brain microvessels; this sequestration causes mechanical microvessel obstruction, blood flow reduction, hypoxia, coma, and death (Baptista et al., 2010; Strangward et al., 2017). Furthermore, this exacerbates an inflammatory response in glial cells, with the release of pro-inflammatory cytokines and chemokines such as tumour necrosis factor (TNF-α) and C-X-C motif chemokine ligand-10 (CXCL-10) both of

* Corresponding author at: CIIL, Team 4, Institut Pasteur de Lille, 1 rue du Professeur Calmette, F-59019 Lille sedex, France.
E-mail address: sylviane.pied@pasteur-lille.fr (S. Pied).
[1] These authors contributed equally.

https://doi.org/10.1016/j.bbi.2023.12.030
Received 4 April 2023; Received in revised form 12 December 2023; Accepted 21 December 2023
Available online 27 December 2023

which are tightly correlated with brain injury in murine and in Human CM as well as *in vitro* models (Dalko et al., 2016; Jain Vet al., 2008; Shrivastava et al., 2017).

This neuroinflammatory pathway promotes the breakdown of the blood–brain barrier (BBB) and infiltration of the central nervous system (CNS) by pathogenic $CD8^+$ T lymphocytes expressing CXCL-10 receptors (CXCR3) (Dominique et al., 2000; Kossod and Grau, 1993; Shaw et al., 2015). We recently reported that *PbA*-derived microvesicles (MVs) promote the inflammatory response of astrocytes via the induction of a non-conventional autophagy pathway involving microtubule-associated protein 1 light chain 3 (MAP1LC3, also known as LC3) (Leleu et al., 2021).

Along with their role in the maintenance of brain homeostasis and BBB integrity, glial cells act as primary innate immune effector cells involved in many pathophysiological changes in the CNS (Alireza Minagar et al., 2002; Benarroch, 2013; Khakh and Sofroniew, 2015). Glial cells promote inflammation in neurodegenerative diseases by contributing to a chronic impairment in the production of pro-inflammatory factors (Baker and Petersen, 2018). It is well known that astrocytes induced into senescence have a number of detrimental effects, such as glutamate excitotoxicity, impaired synaptic plasticity, neural stem cell loss, and BBB dysfunction (Cohen and Torres, 2019). More generally, the accumulation of senescent cells in tissues and organs and accelerated telomere attrition are involved in many human diseases related to ageing, neurodegeneration, and dementia (Wang et al., 2020). Telomere attrition and the expression of cyclin-dependent kinase inhibitor 2A (CDKN2A, also known as p16) have been observed in blood cells from patients within three months of the onset of *P. falciparum* malaria (Asghar et al., 2018). The presence of shortened telomeres has also been observed in the tissues of *P. ashfordi*-infected birds and was associated with a shorter lifespan (Asghar et al., 2015; Asghar et al., 2016). Lastly, it was recently reported that a low level of *P. falciparum* parasitaemia accelerates cellular senescence in the peripheral blood cells via inflammation and a redox imbalance; these variables normalized after successful treatment and clearance of the parasites (Miglar et al., 2021).

Cellular senescence is a cell state primarily characterized by a prolonged cell cycle arrest induced by cellular stress. It has recently emerged as a fundamental ageing mechanism and contributes notably to diseases in later life (Childs et al., 2017). This phenomenon is usually associated with unrepaired DNA damages, including shortened and deprotected telomeres, epigenetic alterations, oxidative damage, endoplasmic reticulum stress, autophagic activity, and apoptosis resistance (Hernandez-Segura et al., 2018; Pluquet et al., 2015). The biomarkers of the senescence-associated cell cycle arrest include the activation of the DNA Damage Response (DDR) pathway, leading to the stabilisation and phosphorylation of the tumor suppressor protein TP53 (p53), and the elevated expression of the cyclin-dependent kinase inhibitor p21 (encoded by *CDKN1A*), and the hypophosphorylation of the tumor suppressor protein RB (retinoblastoma protein). Alternatively, or in addition, the expression of the cyclin-dependent kinase inhibitor p16 (encoded by *CDKN2A*) can also be increased, leading to the hypophosphorylation of RB as well. The p38MAPK, a member of the stress-activated protein kinase (SAPK) family, is also frequently activated by phosphorylation. Another main marker of senescence is the increase in the lysosomal β-Galactosidase activity, called the senescence-associated β-galactosidase (SA-β-Gal) activity (Abbadie et al., 2017). Furthermore, senescent cells develop a specific secretome known as the senescence-associated secretory phenotype (SASP), which is characterized by high levels of pro-inflammatory cytokines, growth factors, and matrix remodelling enzymes (Coppe et al., 2010). All these senescent cell hallmarks are mechanistically interconnected and could have deleterious consequences, notably by increasing pro-inflammatory cells and factors in the tissue microenvironments (Birch and Gil, 2020).

In the present study, we looked at whether the cellular senescence of astrocytes and microglial cells was involved in the brain inflammation seen in *Pb*A-infected, CM-susceptible (CM^S) C57BL/6JR mice (compared with inflammation free, CM-resistant (CM^R) C57BL/6 WLA-*Berr2* mice) and in cohorts of *P. falciparum*-infected humans with severe malaria (compared with CM-free humans having undergone acute malaria only). We assessed the expression of cellular senescence markers and a panel of inflammatory cytokines *in vivo* in the brain and *in vitro* in primary glial cell cultures. We then studied the mechanisms underlying the induction of cellular senescence by the *Pb*A-astrocyte interaction. Lastly, we evaluated the relationship between cellular senescence, pro-inflammatory cytokine networks and CM in post-mortem blood and brain tissue samples from *P. falciparum*-infected patients.

2. Material and methods

2.1. Primary astrocytes cell culture & parasite stimulation

Primary glial cells were gently dissociated and isolated from the brains of 1–2 days old newborn C57BL/6 mice and cultured *in vitro* as described previously (Shrivastava et al., 2017). Cultures were enriched in astrocytes by gentle shaking during 24 h and kept in DMEM (complete Dulbecco's modified eagle medium; [Gibco, 11,885–084] containing 10 % fetal bovine serum (FBS; [Dutscher, S181B-500]). *Pb*A-iRBCs were recovered from severe combined immune deficiency mice (SCID mice; Institut Pasteur de Lille) as described in (Leleu et al., 2021). *Pb*A-iRBCs were put in contact with astrocytes at a ratio of 10:1 during 24 h and removed. Then, fresh medium was added and culture kept for further, 4,7,10 or 15 days post-stimulation. Non-stimulated astrocytes were cultured in the same conditions and used for controls. For autophagy inhibition, the astrocyte cultures were treated with 10 nM Bafilomycin A_1 (BAF A_1; MedChemExpress, HY-100558) from the beginning of the *Pb*A-iRBCs stimulation to 10 days post-stimulation.

2.2. Animal studies

8–10 weeks old male and female C57BL/6 mice (Janvier laboratories, C57BL/6JR) and B6.WLA-*Berr2* congenic mice, developed in our Lab (Keswani et al., 2020), were kept in standard conditions in the animal facility of the Pasteur Institute of Lille. All mice experiments were performed following institutional guidelines for animal care and use. The study was approved by the French Committee for Animal Health Care "Ministère de l'Agriculture et de la Pêche" n° #22021–2019091715283871. Mice were infected intraperitoneally using 10^6 RBCs infected by *Pb*A, clone 1.49L. Same age non-infected mice were used as negative controls. Between 6 and 10 days post-infection, C57BL/6 infected mice developed neurological symptoms unlike C57BL/6.WLA-*Berr2* which did not develop cerebral symptoms but died later from hyperparasitemia. Mice were monitored twice daily following infection. Parasitemia was determined by Giemsa-stained blood smears from the tail vein every three days. All mice were euthanized between days 6 and 8 post-infection. Brains, spleens and sera samples were collected, processed and stocked for the analyses detailed below. For Treatment with senolytic drugs, CM^S mice were treated by oral gavage from day 2 to 8 post-infection with 5 mg/kg Dasatinib (Sigma,SML2589) and 50 mg/Kg Quercetin (Sigma, Q4951).

2.3. Clinical samples procurement and inclusion criteria

Patients sample collection was done during a study evaluating immune responses in malaria severity conducted at SCB Medical College and Hospital, Cuttack, Odisha, between 2008 and 2011 as published (Hernandez-Segura et al., 2018). Patients were categorized according to the World Health Organization (WHO) as follows: Patients with uncomplicated Mild Malaria (MM) and patients with severe malaria (SM). SM patients were categorized into MOD (Multiple Organ Dysfunction), CM (Cerebral Malaria) and CM-MOD (Hernandez-Segura et al., 2018). Thirty-seven patients were investigated in this study: 11 patients with MM, 5 patients with MOD, 14 patients with CM and 7 patients with CM-

MOD (Table 1). No age difference in clinical severity was observed and the severity of the disease was uniformly spread over both genders. *P. falciparum* infection was screened by immune chromatography test (SD Bio Standard Diagnostics, India) and Giemsa stained blood smears as previously described (Herbert et al., 2015). Post mortem Formalin-fixed Paraffin-embedded (FFPE) human brain tissue were obtained from patients who died from CM and from non-infected controls who died from road accident in Ivory Coast. The protocol was reviewed and approved by the Comité National d'Ethique et de Recherche de Côte d'Ivoire (N°56/MSLS/CNER-dkn). Written informed consent was obtained from parents. Brain sections were used to evaluate GFAP and p21 expression in astrocytes by confocal microscopy. The study was done according to the guidelines in the Declaration of Helsinki. In India, it was approved by the National Health Office Ethics committee, the Institutional Human Ethics Committee of SCB Medical College, Cuttack, and the Institutional Review Board of Institut Pasteur de Lille, France. In Ivory coast, samples were collected at the Institute of Forensic Medicine-Faculty of Health, University Félix Houphouët-Boigny of Abidjan, in accordance with the local laws and regulations, International Conference on Harmonization - Good Clinical Practice (ICH-GCP).

2.4. Cell sorting for isolation of brain astrocytes

Single-cell suspensions were obtained from the mice brains, using the Neural Tissue Dissociation kit (Milteny Biotec, 130–093-231). Cells were then stained with anti-ITGAM/CD11b (eBioScience, 12–0112–81) and anti-SLC1A3/GLAST (Miltenyi Biotec, 130–095–814) fluorescent antibodies. Astrocytes ITGAM/CD11b^{-} (integrin alpha M) SLC1A3/GLAST^{+} (solute carrier family 1 (glial high affinity glutamate transporter), member 3) were further sorted on a FACSAria (Becton Dickinson) and analyzed by RT-qPCR, as described previously (Keswani et al., 2020).

2.5. Affymetrix GeneChip analysis

Total RNAs were extracted from the cell lysates of the brains of control and *Pb*A-iRBCs infected CM^{S} and CM^{R} mice using a Trizol® Plus RNA Purification Kit (Invitrogen, 15596026) according to the manufacturer's instructions. As previously described, we used the Affymetrix GeneChip® 1.0 ST Array Mouse (Keswani et al., 2020).

2.6. Quantitative real-time PCR

Total RNAs were extracted by using the Nucleospin RNA kit (Machery Nagel, 740,955,250). Complementary DNA (cDNA) synthesis was done using the SuperScript VILO kit (Invitrogen, 11,754,250) as previously described (Dalko et al., 2016). Then, RT-qPCR was performed by mixing cDNA with primers (Table S1 for mice and S2 for human) (Eurogentec) and SYBR Green Master Mix (ThermoFisher Scientific, 4,385,612). RT-qPCR was done in Quantstudio^{TM} 12 K Flex Real-Time PCR system (ThermoFisher Scientific). Relative expression of genes of interest was quantified using the ΔΔCt or ΔCT (for the human cDNA samples) methods. Data were normalized to *Hprt1* (Hypoxanthine Phosphoribosyltransferase 1) or *Gapdh* (Glyceraldehyde 3-phosphate dehydrogenase) gene expression and expressed as fold-change of gene expression compared with the control condition.

Table 1
Distribution of *P. falciparum* infected patients according to disease profile.

	MM	CM	MOD	CM-MOD	pvalue[1]
N	11	14	5	7	-
% females/% males	18.2/ 81.8	28.6/ 71.4	20.0/ 80.0	14.2/ 85.7	0.87
range of age(years)	20–45	15–65	16–55	15–16	–
mean of age ± 95 % CI (years)	30.8 ± 5.4	30.6 ± 8.5	32.6 ± 18.3	38.4 ± 15.7	0.59

[1] Chi^{2} testfor gender; Kruskal-Wallis test for age.

2.7. Western blot analysis

Brain lysates from CM^{S} and control mice were prepared using lysis buffer (RIPA lysis buffer, Interchim, R0278) containing a Protease Inhibitor Cocktail (Roche, 04693159001). The total protein concentration was measured with the BCA (bicinchoninic acid assay) protein assay kit (Interchim, UP40840A), and 1 mg/mL of protein was used. Then, protein extracts were separated on a standard SDS-PAGE (sodium dodecyl sulfate–polyacrylamide gel electrophoresis) in 5, 10, or 15 % polyacrylamide gels (BioRad) and electro-transferred onto 0.2 μm nitrocellulose membranes (ThermoFisher Scientific, 88,018). Membranes were blocked for 2 h at RT with PBS (phosphate-buffered saline)-0.2 % Tween 20® (Euromedex, 2001-B) and then incubated overnight at 4 °C with the primary antibodies, diluted in PBS-0.2 % Tween 20®, using a Cassette Miniblot System (Immunetics, Interchim). Details of the primary antibodies used are listed in Table S3. After two washes with PBS-0.2 % Tween 20®, the immunoreactivity profile was detected by incubating the membrane with the secondary antibodies (Table S4) diluted in PBS-0.2 % Tween 20®for 2 h. Blots' revelation was done using the Clarity^{TM} Western ECL Substrate (Bio-Rad, 170–5061). Blots' images were captured and analyzed by the Molecular Imager ChemiDoc^{TM} XRS + system (Bio-Rad) using Image Lab^{TM} software (Version 5.2, Bio-Rad). The protein levels and ratio of phosphorylated form and total protein were determined by densitometry using the ImageJ/FIJI software (version 1.53, ImageJ^{TM} software, National Institutes of Health). The protein levels in the CM^{S+} brain were compared to the brain control protein levels.

2.8. Staining, imaging and image processing

Immunofluorescence staining was performed as described elsewhere with little modifications (Vazquez-Villasenor et al., 2020). Serial coronal brain sections from optimal cutting temperature compound (OCT) embedded tissue of control and CM^{S+} mice were cut at 5-μm thickness and spread onto Super-frost Plus slides (ThermoFisher, J1820AMNZ). Paraffin-embedded sections derived from brain of healthy and CM patients were deparaffinised in xylene and rehydrated in alcohol gradient series (Shan-Rong et al., 1991). Astrocyte cultures were processed for confocal microscopy as described previously (Leleu et al., 2021). Sections were then fixed for 10 min for brain and 20 min for cell culture in 4 % paraformaldehyde (PFA, Electron Microscopy Sciences, 15,713 R7G5). Following permeabilization with 0.1 % Triton X-100 (Sigma-Aldrich, T8787), slides were blocked with 5 % FBS for 30 min at RT and incubated overnight at 4 °C with anti-GFAP antibody and followed separately by anti-p21, anti-pp53,anti-Bcl-xl, anti-LC3 or CXCL-10 antibodies (Table S3) diluted in blocking solution. After three PBS 1X washes, appropriate secondary antibodies (Table S4) diluted in 5 % FBS were then incubated for two hours for brain sections or 30 min for cell culture at RT. All slides were incubated, after three PBS 1X washes, with 0.01 mg/ml of DAPI (Invitrogen, D1306) for cell nucleus staining. Finally, the sections were washed and mounted onto glass slides using mounting medium. SA-β-gal activity detection was performed as described (Debacq-Chainiaux et al., 2009). Briefly, coronal brain sections and astrocyte cultures were fixed with 2 % formaldehyde (Sigma, F1268)-0.2 % glutaraldehyde (Merck, 432VV351439) for 5 min then incubated with incubated with 1 mg/ml of 5-Bromoo-4-chloro-3-indolyl β-D-galactoside (X-Gal) (Euromedex, EU0012-D) overnight at 37 °C as previously described. Brain sections were scanned by the Zeiss LSM710 confocal microscope (ZEISS microscopy GmbH) using an Airyscan super-resolution module (0.325 μm/pixel) with a 20X oil immersion lens.

For imaging, fluorescent slides were scanned using the Zeiss AxioScan.Z1 slide scanner (Zeiss, Jena, Germany) using 20x magnification

(0.22 μm/pixel) and auto-estimated exposure times. The whole slide scan was imaged using 4 epi-fluorescent filters (DAPI, Alexa 488, Cy3, Cy5). Images were complemented with image deconvolution using Huygens Essential software (Scientific Volume Imaging, https://svi.nl/). Then, segmentation of individual cells is finally performed by the Imaris Surface creation module (v9.1.2, BitPlane,https://www.bitplane.com) to extract data for quantitative analysis. For SA-β-Gal staining on brain sections, the "% area" results were used as the stained level of SA-β-gal as previously described using ImageJ software (Lozano-Gerona and Garcia-Otin, 2018; Tominaga et al., 2019). Percentage of SA-β-Gal$^+$ cells in stimulated astrocytes was determined manually.

2.9. siRNA silencing

Astrocytes were plated in 12-well plates at 5.10^5 cells/well and then transfected 6 h with *Rubcn/Rubicon* or *Atg5* siRNA (Horizon Discovery; Dharmacon; RUBCN/rubicon 100,502,698; ATG5 11,793) at 25 nM using the HiPerfect transfection reagent (Qiagen, 301,704) and then stimulated with *Pb*A-iRBCs as described in (Leleu et al., 2021).

2.10. Cytokines/chimiokines quantification.

Cytokines and chemokines were quantified in sera of control and *Pb*A-infected CM^S, CM^R and *Pb*A-infected and treated-CM^S mice using ELISA Kits for IL-6 (Biolegend, 431,301), CCL2 (Biologend, 432,704) and CXCL-10 (R&D Systems, DY-466–05) in triplicates.

2.11. Statistics

Statistical analyses and plots were done with R version 1.4.2 (www.rstudio.com). To compare the Affymetrix microarray data between the CM^S and CM^R infected mice we performed a T test and computed an FDR-adjusted p value. When comparing the gene expression levels and the plasma levels between more than two groups, we used the Kruskal-Wallis test followed by a Conover post-hoc test available in the R package PMCMRplus. The p values are Benjamini-Hochberg adjusted. To make graphs, we used ggplot2. ggpubr, ggsignif, rstatix packages and GraphPad Prism (Version 5, GraphPad software, Inc.). The sample size and the number of replicates for each experiment are mentioned in the corresponding figure legend. Analyses of variance for cell culture analysis (ANOVA), followed by Tukey's multiple comparisons or Bonferroni post-hoc tests were used to compare kinetics groups and treatment groups. For survival analyses, we used the log-Rank (Mantel-Cox) test. *P* values, for each experiment were reported as significant as *P < 0.05; **P < 0.01; ***P < 0.001, ****P < 0.0001. To look for relationships between the studied cytokines/chemokines and the markers of senescence we used the software Cytoscape v 3.9.0 and the database STRING for the mouse. An enrichment analysis based on the GO terms and the significantly differentially expressed genes from the transcriptomic data was done with the R package ClusterProfiler. Then p values were adjusted by the false discovery rate method. We used the R package mixOmics to perform the discriminant analysis on the human data.

3. Results

3.1. High expression of markers of cellular senescence and resistance to apoptosis are observed in the brain during ECM

To get insight into the cellular and molecular mechanisms involved in CM pathogenesis, we used C57BL/6JR CM susceptible (CM^S) and B6.WLA-*Berr2* CM resistant (CM^R) mice infected with *Pb*A. We used Affymetrix GeneChip mouse expression arrays to compare whole-brain transcriptomic profiles from CM^S and CM^R *Pb*A-infected and control mice. Of the 1781 genes showing a difference between at least two groups of mice, 660 showed significant differences in expression when comparing CM^S with CM^R mice (false discovery rate (FDR)-adjusted p-value < 0.05). The log2 fold-change ranged from −1.44 to 0.84. In this CM^S vs CM^R comparison, we found that 320 genes were significantly upregulated and 340 were downregulated. Next, we used the R package Cluster Profiler to perform a Gene Ontology (GO) enrichment analysis. Seventy-eight GO terms were found significantly enriched (FDR adjusted p value < 0.05). Of the 141 genes classified in GO's *Mus musculus* senescence pathways (Fig. 1A), we identified three genes (*Cdkn1a/p21, PML* (coding for the promyelocytic leukaemia protein) and *Calr* (coding for calreticulin) that were upregulated in *Pb*A-infected CM^S mice, relative to *Pb*A-infected CM^R mice (Fig. 1B and C). Next, we used real-time qPCR to quantify the mRNA expression levels of four selected senescence biomarkers (*p21*, *GADD45γ*, *p38MAPK* and *p16*) in whole-brain and spleen extracts from non-infected and CM^S and CM^R *Pb*A-infected mice. Significantly greater expression of *p21* (****P < 0.0001), *GADD45γ* (****P < 0.0001) and *p38MAPK* (***P < 0.001) was observed in CM^S brains (Fig. 2A), whereas the expression of *p16* was significantly lower compared to CM^R (**P < 0.01). The presence of a strong link between *p21* up-regulation and CM was suggested by the significant down-regulation of *p21* expression in the brain of *Pb*A-infected CM^R mice (****P < 0.0001); this was also true for *GADD45γ* (****P < 0.0001) and *p38MAPK* (**P < 0.01) (Fig. 2A). Furthermore, the expression of anti-apoptotic genes (such as *Bcl2/1* (*P < 0.05) and *Mcl1* (**P < 0.01)*)* was significantly augmented in infected CM^S mice when compared with control mice, although no difference was observed for *Bcl2/2* and *Bcl2* (Fig. 2B). All these markers were expressed in CM^S brain samples but not in spleen samples (Supplementary Fig. 1). Quantitative western blot analyses of brain extracts from the same mice confirmed the elevated expression of most of the tested proteins in the CM^S brain, relative to non-infected controls: ~1.5-fold for p21 (**P < 0.01), 2-fold for the p-p53/p53 ratio (*P < 0.05) and ~ 2-fold for the p-p38MAPK/p38 ratio (**P < 0.01), (Fig. 2C). Moreover, to determine whether this acquisition of senescence markers was associated with DNA damages, we searched for the phosphorylation of ataxia telangiectasia mutated (ATM), one marker of the activation of the DNA damage response pathway. It is noteworthy that the phospho-ATM (p-ATM)/ATM ratio was higher (***P < 0.01) in the CM^S brain samples (Fig. 2C). Furthermore, we observed a higher proportion of SA-β-Gal-positive cells (a 5-fold difference, *P < 0.05) on frozen coronal brain sections from CM^S mice than on sections from non-infected mice (Fig. 2D). Taken as a whole, these data revealed the presence of senescent cells in brain tissue samples from CM^S mice.

3.2. Astrocytes are the brain cells most affected by senescence during CM

In order to determine which subpopulation(s) of glial cells underwent senescence during ECM, we next used RT-qPCR to quantify the expression of senescence markers by astrocytes and microglial cells in samples of brain tissue from CM^{S+} and CM^R *Pb*A-infected mice. Significantly greater expression of the *p21*, *Gadd45γ* and *Bcl-2/1* genes was observed in astrocytes from CM^S mice but not in astrocytes from CM^R mice or microglial cells isolated from CM^s or CM^R mice (Fig. 3A and B). Immunofluorescence/confocal microscopy assessments of brain sections revealed that the proportion of GFAP$^+$ activated astrocytes expressing p21 among total GFAP$^+$ was higher in the cortex of CM^S mice brain (~40 %) than in the cortex of non-infected controls (~15 %) (Fig. 3C). The proportion of GFAP$^+$ p-P53$^+$ astrocytes was greater in CM^S mice (~36 %) than in non-infected control mice (13 %; *P < 0.05; Fig. 3D). Likewise, the proportion of GFAP$^+$ Bcl-xl$^+$ astrocytes was greater in CM^S mice (~42 %) than in non-infected control mice (<20 %; **P < 0.01; Fig. 3E). It is noteworthy that brain sections from CM^S mice showed SA-β-Gal$^+$ staining in the areas with elevated p21 expression (Supplementary Fig. 2). Thus, the astrocytes appeared to be particularly affected by a p21-mediated senescence process induced by *Pb*A in the brain during CM.

A

NCBI Gene ID	Gene Name	Gene symbol	P-value[1]
12575	Cyclin-dependent kinase inhibitor 1A	Cdkn1a	0.014
18854	Promyelocytic leukemia	PML	0.020
12317	Calreticulin	Calr	0.001

B

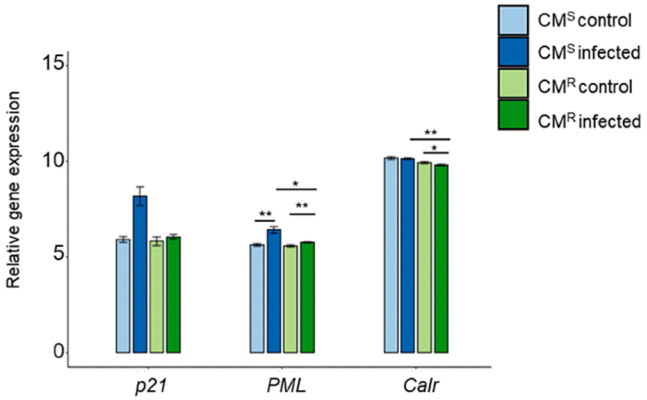

Comparison of the levels of PML in the four groups of mice

	CMR infected	CMR control	CMS infected
CMR control	0.004	-	-
CMS infected	0.045	7.2e-04	-
CMS control	0.024	0.203	0.002

Comparison of the levels of CALR in the four groups of mice

	CMR infected	CMR control	CMS infected
CMR control	0.045	-	-
CMS infected	0.002	0.024	-
CMS control	7.2e-04	0.004	0.203

C

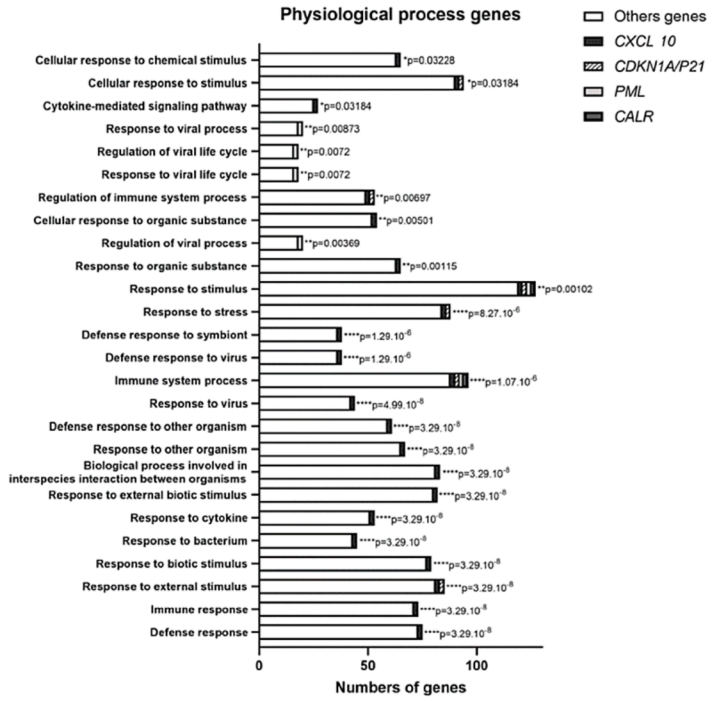

Fig. 1. Transcriptomic senescence signature associated with ECM in the brain. (**A**) Senescence genes upregulated in CM^S compared with CM^R infected mice. [1]p-value obtained when comparing the infected CM^s and CM^R mice using Student's *t*-test. *P < 0.05; **P < 0.01. Relative expression of (**B**) *p21, PML* and *Calr* in the brains of control and infected CM^S and CM^R mice at day 6.5 post infection mades using Affymetrix GeneChip Mouse Expression Arrays. Data represented as mean ± SEM. Groups (n = 3 per group) were compared with a Kruskal-Wallis test, followed by a Conover post-hoc test when significant. P values are adjusted by FDR Benjamini-Hochberg. (**C**) Contribution of senescence genes to physiological processes during ECM. The FDR adjusted p-values come from a Gene Ontology enrichment analysis.

3.3. Astrocyte senescence is triggered by direct interaction with the malaria parasite

To determine the molecular events implicated in the induction of astrocyte senescence, primary culture of astrocytes derived from CM^S mice were incubated *in vitro* with *Pb*A-iRBCs (Fig. 4A). The induction of senescence was monitored by measuring SA-β-Gal activity in primary astrocyte cultures 4, 7, 10 and 15 days after contacting with *Pb*A-iRBCs. From day 4 onwards, the proportion of SA-β-Gal^+ cells were significantly higher in parasite-stimulated cells (~30 %; **P < 0.01) than in non-stimulated cells (~10 %; Fig. 4B). The highest proportions of SA-β-Gal^+ cells were observed on day 10 (~40 %; *P < 0.05) and day 15 (~37 %; **P < 0.01). This SA-β-Gal activity was correlated with morphological changes in astrocytes, such as enlargement of the cytoplasm, a low nucleus/cytoplasm ratio (Fig. 4C), and a rise in the expression of *p21* (***P < 0.001; Fig. 4D) on day 10. A confocal

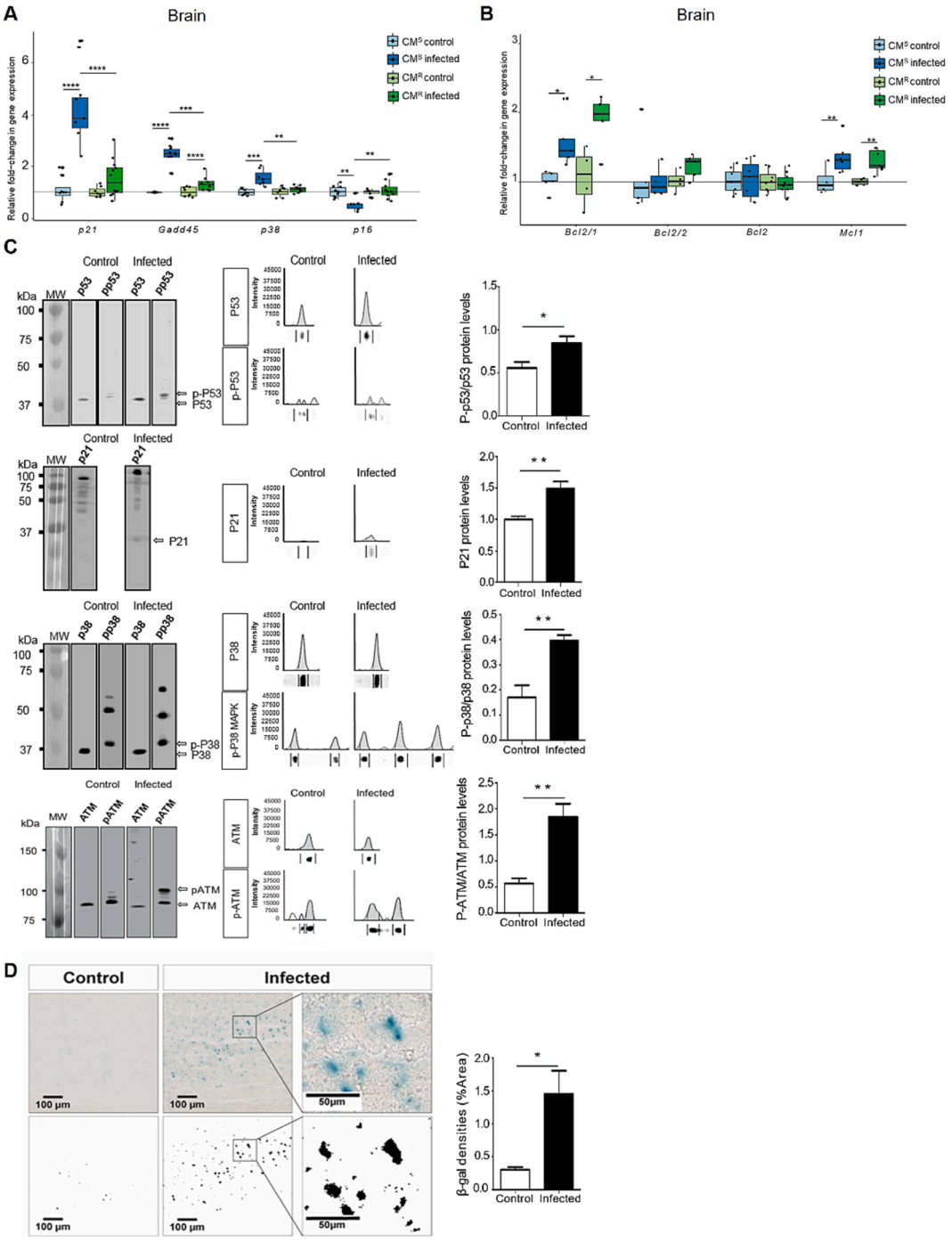

Fig. 2. Expression of senescence markers in the brain during ECM. Fold-relative expression of (**A**) cell cycle arrest genes: *p21^{WAF1}, GADD45γ, p38MAPK* and *p16^{INK4}*. (**B**) anti-apoptotic genes: *Bcl2/1, Bcl2/2, Bcl2 and Mcl1* in whole-brain of control and infected CM^S and CM^R mice at day 6.5 post infection. Data are presented as mean ± SEM. Values (n = 3–10 per group) were compared with the control group or between selected groups using a Kruskal-Wallis test followed by a Conover post-hoc test, *P < 0.05; **P < 0.01; ***P < 0.001; ****P < 0.0001. (**C**) Western blot analysis of phosphorylated and total p53 (phosphorylated on Serine 15), p21^{WAF1}, p38MAPK, ATM proteins in the whole-brain lysates of control and infected CM^S mice. Protein levels were shown as mean ± SEM of at least three independent experiments. The experimental group was compared to the control group using Student's *t*-test (*P < 0.05; **P < 0.01). (**D**) Representative SA-β-Gal staining in coronal brain sections, from control and infected CM^S mice. Scale bars = 100 µm. Data are representative of three independent experiments. The experimental group was compared to the control group, using Student's *t*-test*P < 0.05.

microscopy analysis revealed that the proportion of astrocytes co-expressing GFAP and p21 was 18 % in stimulated cultures and 6 % in non-stimulated control cultures (*P < 0.05) (Fig. 4E). This finding suggests that direct interaction with *Pb*A-iRBCs can induce a p21-senescence-like phenotype in astrocytes.

3.4. *PbA-induced astrocyte senescence is triggered by LC3-dependent, non-conventional autophagy*

We then looked at whether the p21-induced senescence process induced by *Pb*A-iRBCs was linked to the LC3-associated phagocytosis (LAP) evidenced during the transfer and degradation of *Pb*A MVs in astrocytes as we published (Leleu et al., 2021). An immunofluorescence/

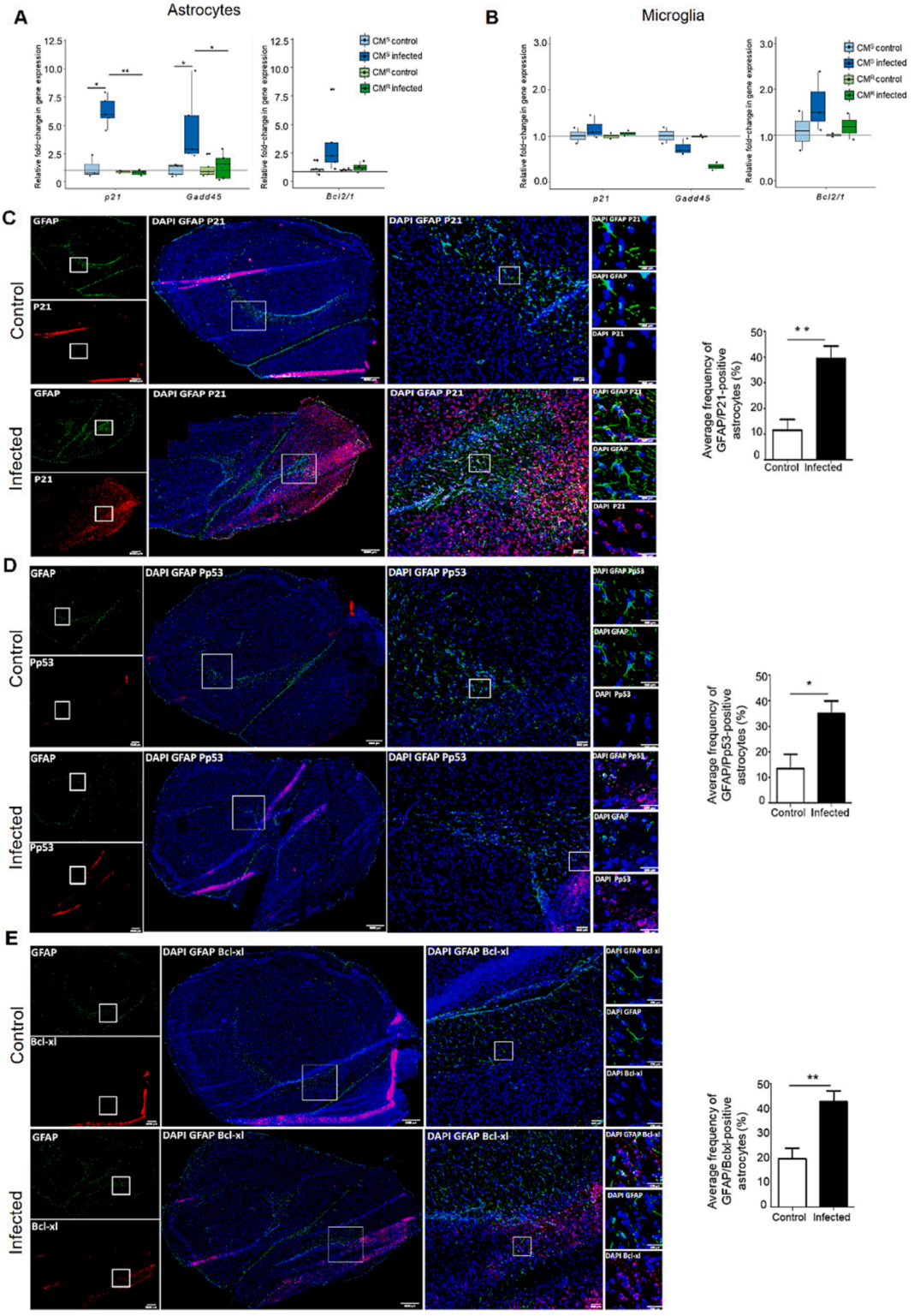

Fig. 3. A senescence-like phenotype of astrocytes during ECM. Relative mRNA levels of *p53*, *p21*^{WAF1}, *GADD45γ* and *Bcl2/1* in the sorted (**A**) Astrocytes and (**B**) Microglia of control and infected CM^{S} and CM^{R} mice at day 6.5 post infection. Values were compared with the control group or between selected groups using a Kruskal-Wallis test followed by a Conover post-hoc test. *P < 0.05; **P < 0.01. Representative immunofluorescence images showing (**C**) p21, (**D**) p-p53, (**E**) Bcl-xl protein levels (red) in GFAP^{+} astrocytes (green) in the brain of infected CM^{S} mice compared with control scale bar represents 2000 μm. White boxes show magnified regions (scale bars, 100 μm). Graphs show quantification of the percentage of activated astrocytes (GFAP + cells) expressing p21 or p-p53 or Bcl-xl. Data are presented as mean ± SEM. Values (n = 5 mice) were compared with the control group using Student's *t*-test. *P < 0.05; **P < 0.01; ***P < 0.001.

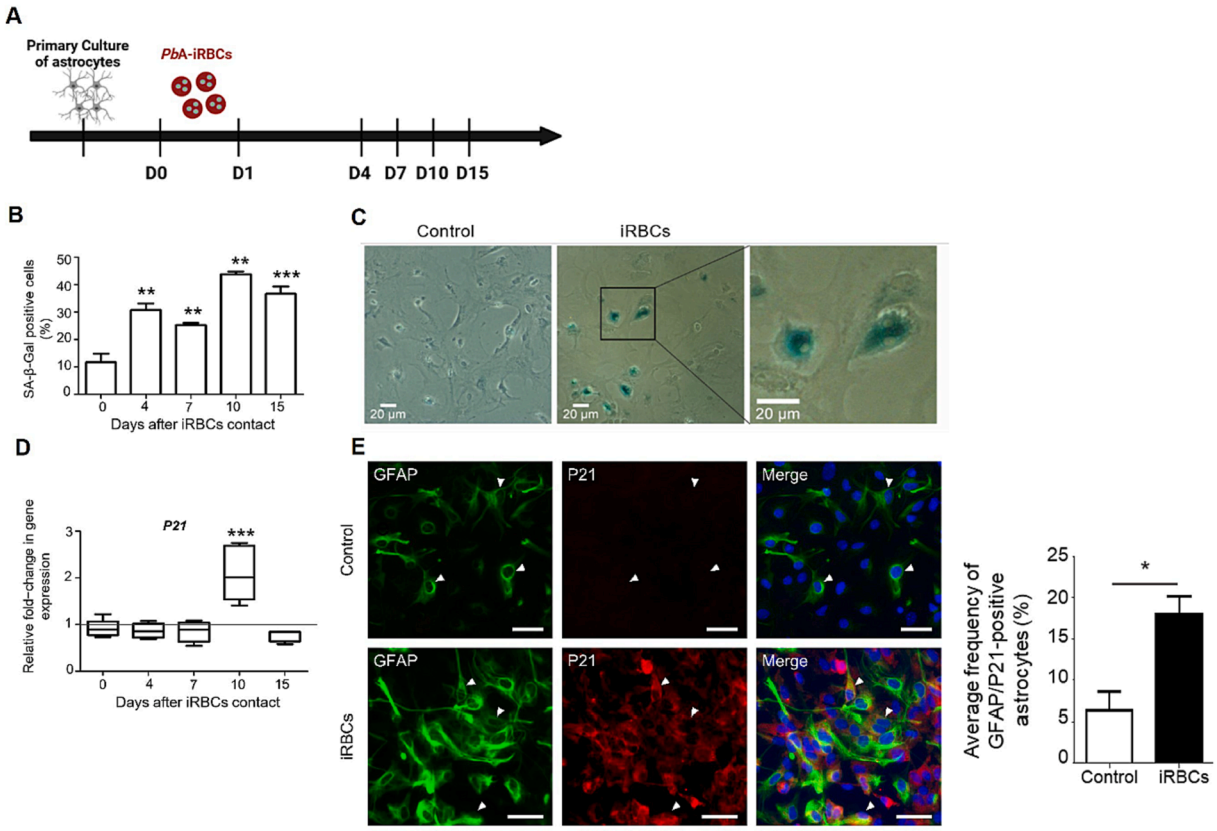

Fig. 4. Astrocytes undergo premature senescence after direct contact with *Pb*A-iRBCs. Primary astrocyte cultures were incubated with *Pb*A-iRBCs at a ratio of 1:10 for 24 h. *Pb*A-iRBCs were removed after 24 h and the astrocytes were incubated further for 4 or 7 or 10 or 15 days. (**A**) Experimental schema of astrocytes *in vitro* stimulation by *Pb*A-iRBCs. (**B**) Quantification of SA-β-Gal-positive astrocytes at 0, 4, 7, 10 and 15 days post-stimulation (n = 3–5 per condition). (**C**) Representative images of SA-β-Gal staining in astrocytes stimulated or not with *Pb*A-iRBCs at day 10 (Scale bar: 20 µm). (**D**) Relative p21^{WAF1} gene expression at different time points post-stimulation by *Pb*A-iRBCs as compared with non-stimulated controls. (n = 4–7 per group) (**E**) Representative images of double immunofluorescence (white arrows) showing p21 protein levels (red) and GFAP astrocytes (green) in astrocytes stimulated with *Pb*A-iRBCs at day 10 compared with non-stimulated cells. (Scale bar: 20 µm). Percentage of GFAP/P21 positive astrocytes (n = 3–5 per group). All data are presented as mean ± SEM. Values were compared with the control group using Student's *t*-test. *P < 0.05; **P < 0.01; ***P < 0.001.

confocal microscopy analysis of astrocyte cultures stimulated (or not) with *Pb*A-iRBCs showed GFAP$^+$ astrocytes (in green, in Fig. 5A) co-expressing p21$^+$ (in red) and MAP1LC3/LC3$^+$ (in magenta); the proportion of co-expressing cells was ~ 16 % with *Pb*A-iRBCs and ~ 7 % without (**P < 0.01). To confirm the link between LAP and p21, we used a RNA silencing strategy to target *Rubcn/Rubicon* and *Atg5*; the latter are known to be essential for the LAP of *Pb*A MVs by astrocytes (Leleu et al., 2021). After silencing *Rubcn* and *Atg5*, the expression of *p21* in cultured astrocytes on day 10 after contact with iRBCs was 2 fold-change decreased (Fig. 5B). The same was true for the expression of *Rubcn* and *Atg5, but less for Map1Lc3/Lc3,* in cultures treated with si*Rubcn* and si*Atg5*, compared with an iRBC-stimulated control (Fig. 5B). No effect on *p16^{INK4}* expression was observed after si*Rubcn* treatment. We also used confocal microscopy to study the effects of the autophagy inhibitor bafilomycin A_1 (BAF A_1) on *Pb*A-induced senescence in astrocytes. The proportion of GFAP$^+$ and P21$^+$ astrocytes was lower in BAF A_1-treated cultures (~5%; **P < 0.01) than in non-treated, *Pb*A-stimulated cultures (~20 %; Fig. 5C). Taken as a whole, these data strongly suggest that autophagy is linked to the senescence processes induced by the astrocyte-*Pb*A interaction.

3.5. *Parasite-induced senescence is correlated with the production of pro-inflammatory cytokines/chemokines by astrocytes*

CXCL-10 is one of the main pro-inflammatory factors found to be significantly overexpressed in the brain of CM^S infected mice (relative to controls), as evidenced by transcriptomics experiments (Fig. 6A) and RT-qPCR quantification (Fig. 6B). We also observed high levels of *Cxcl-10* gene expression in *ex vivo* astrocytes isolated from CM^S brain (compared CM^R mice; Fig. 6C) and plasma (Fig. 6D); this finding attested to the astrocytes' involvement in the neuroinflammatory response to ECM. Immunofluorescence/confocal microscopy analyses of brain sections from CM^S and control mice labelled with DAPI (in blue) and anti-GFAP (in green), anti-CXCL-10 (in magenta) and anti-p21 (in red) antibodies showed that the proportion of activated GFAP$^+$ astrocytes co-expressing p21 and CXCL-10 was 36 % in CM^{S+} mice and 4 % in non-infected control mice (**P < 0.01) (Fig. 6E). Following on from our recent observation whereby CXCL-10 secretion by *Pb*A-iRBC-stimulated astrocytes from CM^S mice is associated with LC3 non-canonical autophagy (Leleu et al., 2021), we next looked at whether CXCL-10 secretion by senescent astrocytes is linked to autophagy in primary astrocyte cultures treated with bafilomycin A_1 (BAF A_1). Ten days after contact with *Pb*A-iRBC, the proportion of GFAP$^+$P21$^+$astrocytes producing CXCL-10 (in magenta: ~14 %) was significantly greater than in non-stimulated cells (~2.8 %; *P < 0.05). There was no difference between control cell cultures treated with BAF A_1 (~2%) and non-stimulated cells (Fig. 6F). These data were confirmed in experiments performed 10 days after the stimulation of primary astrocyte cultures and *Rubcn* and *Atg5* silencing: *Cxcl-10* expression was downregulated with si*Rubcn* (*P < 0.05; Fig. 6G). There was no difference between control stimulated astrocytes or those with *Atg5* silencing alone (Fig. 6G). Furthermore, p21-dependent senescence interactions between

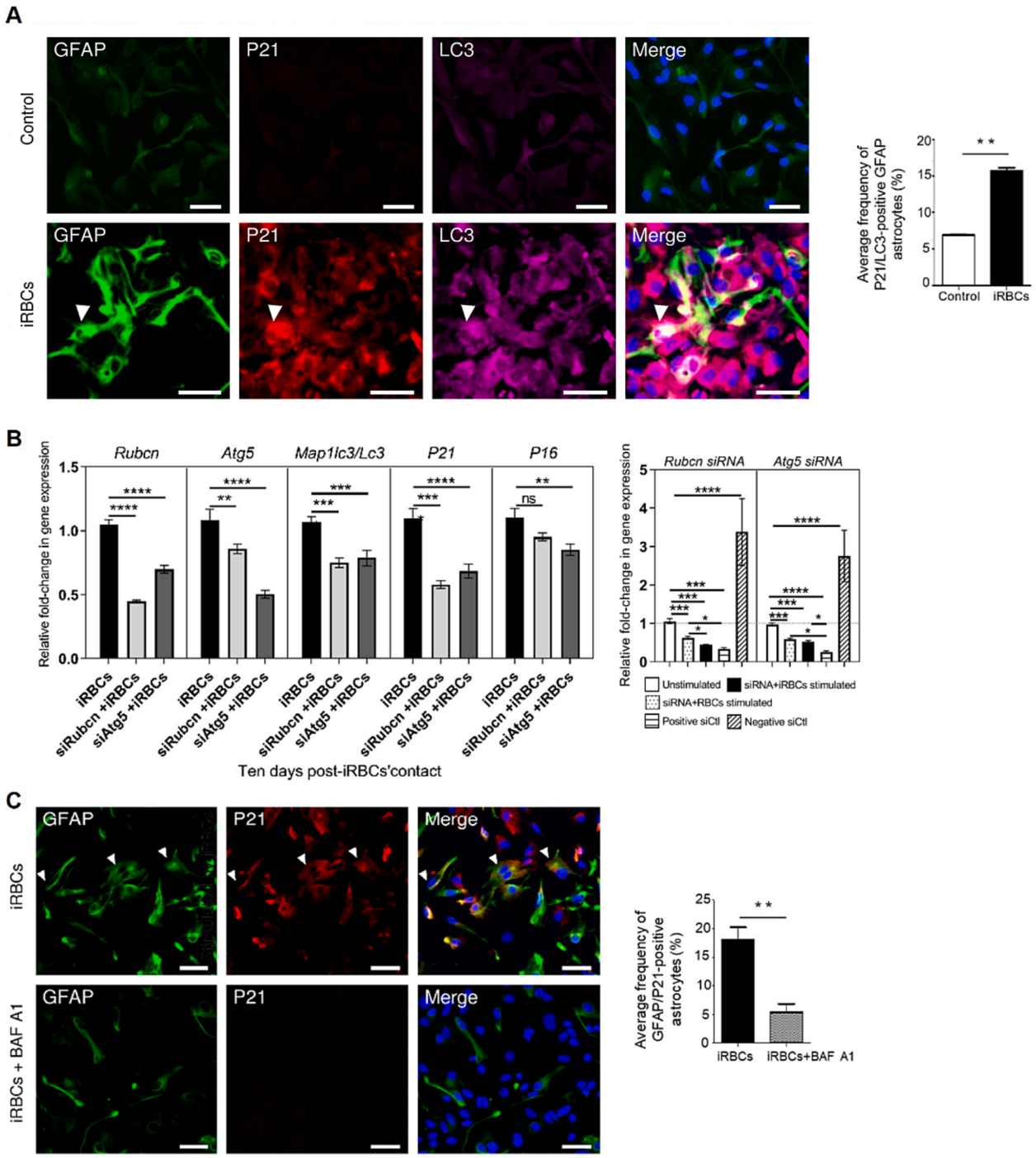

Fig. 5. Autophagy promotes astrocyte senescence after contact with *Pb*A parasite. Primary astrocyte cultures incubated with *Pb*A-iRBCs were transfected or not with 25 nM *siRubcn/Rubicon* or si*Atg5* RNA from the time of contact to 10 days. (**A**) Confocal imaging stimulated and non-stimulated controls astrocytes at day 10, GFAP (green), p21 (red) and LC3 (magenta). (Scale bar: 20 μm). Data are presented as mean ± SEM. The experimental condition (n = 2–5 per group) was compared to the control using Student's *t*-test **P < 0.01. (**B**) Relative expression of *Rubcn*, *Atg5*, *Map1lc3/Lc3*, *p21* and *p16* genes in non-treated, si*Rubcn/Rubicon*-, and si*Atg5*-transfected astrocytes at 10 days after stimulation by *Pb*A-iRBCs (n = 3–5 per group). Uninfected RBCs (RBCs) were as control of parasite stimulation. Data are mean fold-change ± SEM of genes expressed. **P < 0.01; ****P < 0.0001. (**C**) Confocal imaging of astrocyte cultures stimulated and treated or not with 10 nM of BAF A_1 (Scale bar: 20 μm). Data are presented as mean ± SEM. Values (n = 2–5 per group) were compared with the infected non-treated group using Student's *t*-test **P < 0.01.

p38, *p53*, *p21* and *CXCL-10* expressed in the brain of CM^S mice were also revealed by an analysis of the Search Tool for the Retrieval of Interacting Genes/Proteins (STRING) database (Fig. 7A). CXCL-10, p21 and LC3 were positively associated but did not reach the statistical significance (Fig. 7B). The production of two other pro-inflammatory factors (interleukin (IL)-6 and Ccl-2) was also greater *ex vivo* in astrocytes isolated from the brain of CM^S mice and *in vitro* after *Pb*A stimulation (Supplementary Fig. 3). We observed interactions between senescence factors (such as P38 and P53) and two pro-inflammatory factors (IL-6 and CCL2) (Fig. 7A). The fact that *IL6* and *CCL2* expression was elevated in *Pb*A-stimulated astrocytes silenced for *Rubcn* suggested that IL-6 and CCL2 production was not related to LAP (Supplementary Fig. 4). These

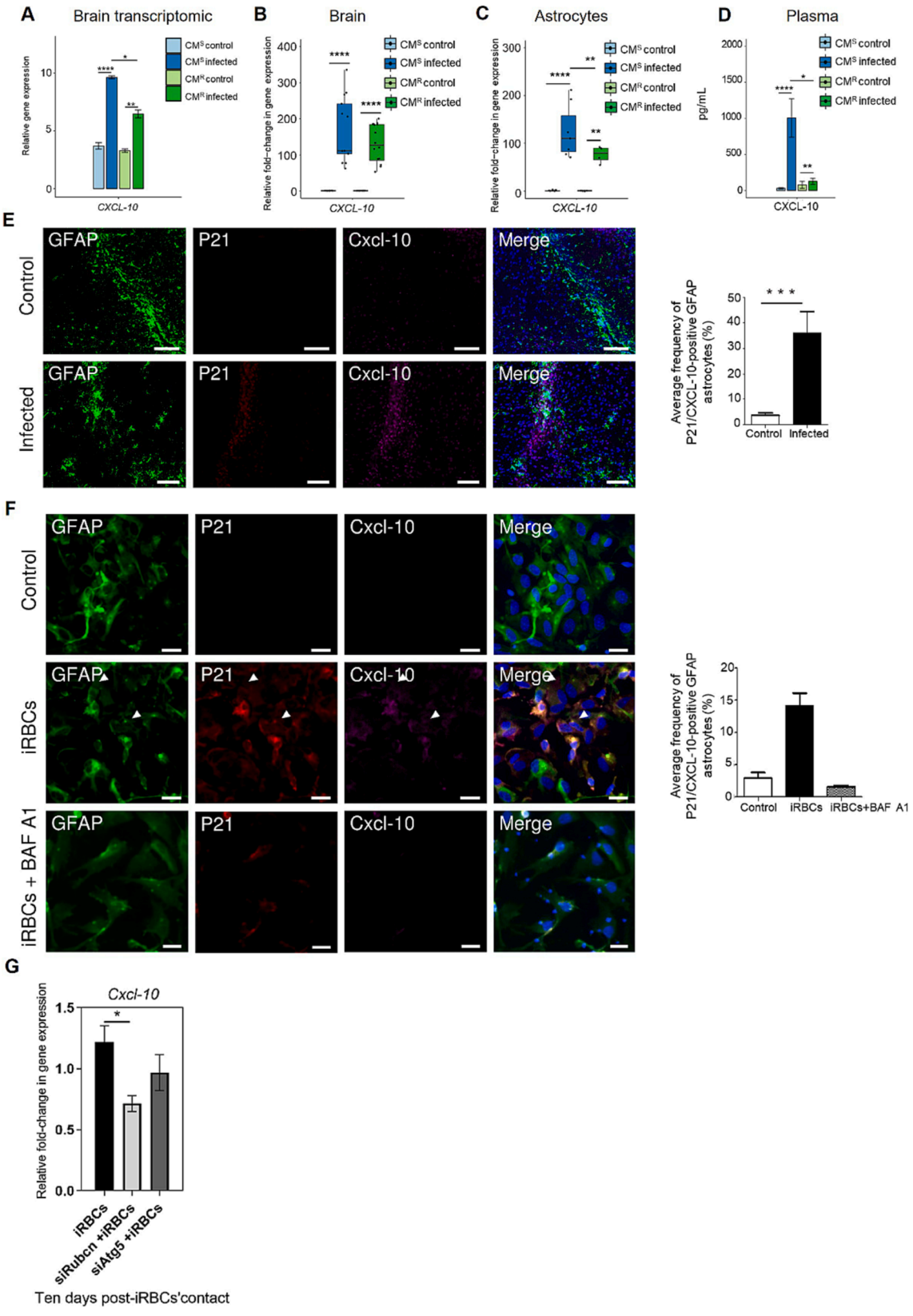

(caption on next page)

Fig. 6. Senescent astrocytes secrete CXCL-10 during ECM. (**A**) Relative expression of CXCL-10 in the brains of mice using Affymetrix GeneChip Mouse Expression Arrays at day 6.5 post infection. Statistics data are indicated in the Table S5. (**B**) Relative expression of *CXCL-10* genes in the brains of control and infected CM^S and CM^R mice (n = 11–16 per group) (Statistics data are indicated in the Table S5) and in (**C**) the sorted astrocytes (n = 4–7 per group). (**D**) CXCL-10 plasma levels measured by ELISA (n = 5 per group). Groups were compared with a Kruskal-Wallis test followed by the Conover post-hoc test when significant. P values are adjusted by FDR Benjamini-Hochberg (Table S5). (**E**) Representative immunofluorescence images showing p21 (red) and CXCL-10 (magenta) protein levels in $GFAP^+$ astrocytes (green) in the brain of infected CM^S mice compared with control. Scale bar = 2000 μm. Graphs show quantification of the percentage of GFAP/P21/CXCL-10 positive astrocytes (n = 3 per group). Data are presented as mean ± SEM. Experimental condition was compared to the control group using Student's *t*-test **P < 0.01. (**F**) Confocal immunofluorescence images of the labelling for GFAP astrocytes (green), p21 (red) and CXCL-10 (magenta) in stimulated astrocytes treated or not with BAF1 A_1, compared with that of non-stimulated cells (Scale bar: 20 μm). Graphs show quantification of the percentage of GFAP/P21/CXCL-10 positive astrocytes. Data are presented as mean ± SEM. experimental condition (n = 2–5 per group) was compared to the infected non-treated group using Student's *t*-test *P < 0.05; **P < 0.01. (**G**) Relative *CXCL-10* gene expression levels in non-treated, si*Rubcn/Rubicon*-, and si*Atg5*- transfected astrocytes at 10 days after stimulation by *Pb*A-iRBCs (n = 3–5 per group). Data represent median fold-change ± SEM of genes expressed. Statistical analysis was performed using one-way ANOVA with Dunnett's multiple comparisons post-test, with data considered significant at *P < 0.05.

data strongly suggest that CXCL-10 secretion by senescent astrocytes depends (at least in part) on the autophagy of *Pb*A-MVs.

3.6. Treatment with senolytic drugs prevents the accumulation of senescent astrocytes in the brain and blocks the onset of ECM by reducing the inflammatory response

To confirm the impact of astrocyte senescence on the pathophysiology of ECM, we treated CM^S mice with a mixture of the senolytic drugs dasatinib and quercetin after infection (Fig. 8A). Based on our data, we believe that this dasatinib-quercetin (DQ) mixture would eliminate senescent cells by inducing apoptosis in the brain of ECM (Zhang et al., 2019a). After oral administration of DQ to CM^S mice from day 2 to 8 post-infection, 60 % of the mice survived (**P < 0.01) (Fig. 8B). However, mice died of hyperparasitaemia 30 days following the infection (Fig. 8C). The parasitaemia was not affected by the DQ treatment (Fig. 8C). The mRNA expression of $p21^{WAF1}$ (**P < 0.01), *GADD45γ* (*P < 0.05), and *pRB* (*P < 0.05) was lower in treated mice than in control mice suggesting the clearance of senescent astrocytes in the treated group. No significant differences were noted for *p38MAPK* and *p16* (Fig. 8D). In line with these observations, the percentage of $GFAP^+$ activated astrocytes expressing p21 on brain sections was lower in infected, treated mice (~28 %) than in infected, non-treated mice (~40 %; *P < 0.05; Fig. 8E). We next evaluated the impact of the two senolytic drugs on the inflammatory response induced in the brain after infection, by quantifying CXCL-10 expression. *Cxcl10* gene expression in the brain was significantly lower (*P < 0.05) in infected, treated mice than in infected, non-treated mice (Fig. 8F). This difference in expression was associated with significantly lower serum CXCL-10 levels (****P < 0.0001) in infected, treated CM^S mice (Fig. 8G). Altogether, these data suggest that the inflammatory response during ECM is associated with the astrocyte senescence.

3.7. Relevance to p. Falciparum-induced human CM

We extended our study to humans by assessing p21 expression (using confocal microscopy) in the brains of patients from the Ivory Coast who had been infected with *P. falciparum* and had died of CM. In line with our findings in the mouse, the percentage of activated astrocytes expressing $GFAP^+p21^+$ was higher in brain samples from the CM patients (~27 %) than in samples from healthy individuals (~15 %; **P < 0.01; Fig. 9A). Furthermore, we detected sequestered *P. falciparum* iRBCs in the microvasculature of the same brain regions (Fig. 9B). Next, we used RT-qPCR to quantify the mRNA expression of $p21^{WAF1}$ and $p16^{INK4}$ in total peripheral blood mononuclear cells (PBMCs) from patients from India with mild malaria (MM), isolated CM, multi-organ failure (MOD) and (CM-MOD). We observed significantly greater expression of $p21^{WAF1}$ in the CM (*P < 0.05) and CM-MOD groups (*P < 0.05), relative to the MM group (Fig. 9C). The difference in p16 expression between the MM and -MOD groups was not significant (Fig. 9D). However, the p16 expression in the CM group (*P < 0.05) and the CM-MOD group (*P < 0.05) was significantly lower than in the MM group, and there was no difference in p16 expression between the CM and CM-MOD groups (Fig. 9D). These results suggested that p21-driven senescence also occurs in the PBMCs and brain cells of patients who have died of CM.

Lastly, we evaluated the relationship between the expression of the senescence markers p16 and p21 and plasma levels of SASP components, including CXCL-10 (Herbert et al., 2015). To that end, we tested the ability of cytokine and chemokine plasma levels and p21 and p16 expression levels to discriminate between different malaria severity groups among the patients from India. The resulting two-factor representation shown MM, CM and the CM-MOD form distinct groups (Fig. 9E). The parasite load increase was significantly associated with increased risk of death in adult patients from India (Fig. 9F).

4. Discussion

Accelerated cellular aging and a shorter lifespan were observed recently in birds and patients with acute malaria; however, CM patients were not assessed (Asghar et al., 2015; Asghar et al., 2016; Asghar et al., 2018; Miglar et al., 2021). Our present study show that astrocyte senescence possibly induced by malaria parasite that may participate in the neuroinflammatory response during CM in mice and humans. In contrast to the observation in birds infected with *P. ashfordii* (inducing CM that induces senescence in the brain, spleen and other tissues), only astrocytes (and not microglial cells) were seen underwent senescence (Asghar et al., 2016). Our observations corroborate previous reports of the astrocytes' role in age-related neuro-inflammatory disorders and in infectious diseases (Cohen and Torres, 2019). The transcriptomic analyses of total brain extract and the quantification of gene expression in CM^S and CM^R *PbA*-infected mice and the corresponding non-infected controls, allowed to identify a parasite-induced, p53/p21-dependent pathway involved in the astrocyte senescence. These data were confirmed by confocal microscopy and immunofluorescence assessments of p21 expression on brain sections from CMS mice and of primary astrocyte cultures stimulated with *Pb*A-infected RBCs. Furthermore, we extended our findings to humans by highlighting a greater proportion of $GFAP^+$ astrocytes expressing p21 on brain sections from *P. falciparum*-infected patients who had died of CM. P21 expression colocalized with GFAP during astrocyte activation. High levels of P16 and P21 expression have been detected in the frontal cortex during neuroinflammation associated with amyotrophic lateral sclerosis – suggesting the presence of cell cycle dysregulation and the activation of astrocyte senescence in the early stages of the disease (Vazquez-Villasenor et al., 2020). These mechanisms were associated to the DNA damage response (DDR) triggering (Vazquez-Villasenor et al., 2020). Even though the brain cortex undergoes major molecular and functional changes with age, the ratio between percentage of p21-positive cells and p16-positive cells is stable over a broad spectrum of ages in people free of neurological disorders; hence, p21 overexpression appears to be related to a neuro-inflammatory process (Idda et al., 2020). Another recent study demonstrated that the S1 subunit of the spike protein from SARS-CoV-2 induces endothelial senescence, as characterized by the expression of both p16 and p21; this senescence might impair the function of brain vessels and

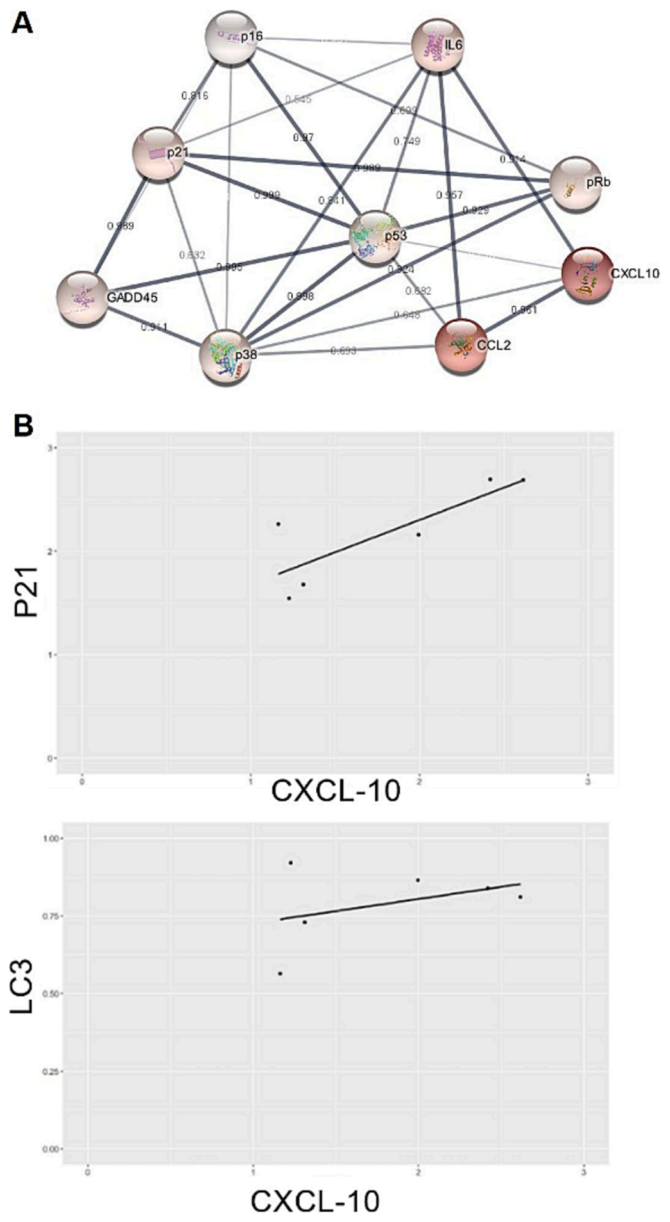

Fig. 7. Interaction between cell cycle arrest regulators and SASP factors during ECM. (**A**) Cytoscape analysis, based on the STRING database, showing the interaction between cell cycle arrest genes (p53, p38, p21, pRb, GADD45 and p16) and SASP factors (IL-6, CXCL-10 and CCL-2). The intensity of node coloring reflects the mean level of gene expression in the brain of infected CM^S mice at day 6.5 post infection, the transparency and thickness of the edges are linked to the confidence in the interaction. Confidence scores range below 0.5 are not indicated. **(B)** Relationship between p21 or LC3 and CXCL-10 in *Pb*A stimulated astrocytes *in vitro*.

thus trigger the onset of cerebrovascular disorders like stroke and haemorrhage (Choi et al., 2022). It should be noted that the p16 and p21 pathways could have distinct roles in senescence: p21 seems involved in the initiation of the process, whereas p16 would be required for long-term maintenance of the senescence state (Herranz and Gil, 2018; Rayess et al., 2012). In the context of CM, we also observed higher levels of p53 protein and higher levels of the Ser-15 phosphorylated form of p53, which is known to be induced by ATM, an upstream kinase in the DDR pathway (Haupt et al., 1997). P21 is the main p53 target gene known to elicit a prolonged cell cycle arrest leading to senescence (Rufini et al., 2013). The higher observed levels of phosphorylated ATM and P53 in CM^{S+} mice brains suggest that the DDR-ATM/P53/p21 pathway is involved in regulating senescence during ECM. Astrocyte senescence was also characterized by the canonical cell enlargement, by the increase in SA-β-Gal activity, and by the expression of some secreted proteins characteristic of the SASP.

In our study, the senescent state of astrocytes was associated with the apoptosis resistance, as shown by the significantly elevated expression of *Bcl2/1* (but not that of *Mcl1*, *Bcl2/2* or *Bcl2*) in infected CM^{S+} mice, relative to infected CM^R mice. In fact, the upregulation of the anti-apoptotic protein of the Bcl-2- family, such as Bcl-2, Bcl-xL, Bcl-w or Mcl-1 is one of the molecular mechanism by which senescent cells acquire resistance to apoptosis. The inhibition of Bcl-2-, Bcl-w-w and Bcl-xl proteins causes the preferential apoptosis of senescent cells and a decrease in the proportion of SA-β-Gal^+ cells (Childs et al., 2014; Yosef et al., 2016). This apoptosis resistance makes senescent cells long-lived cells; we propose that this could contribute to the long term sequelae in CM survivors.

We also identified a link between the cellular senescence process and the involvement of LC3-dependent non-conventional autophagy, which is elicited during the transfer of parasite MVs into astrocytes. In fact, the p21-mediated senescence process induced in astrocytes after *Pb*A contact was totally abolished when autophagy was inhibited by either silencing *Rubcn* or *Atg5* with siRNA or treating with BAF A_1. The relationship between these two cellular stress responses (i.e. autophagy and senescence) is complex; depending on the circumstances, autophagy can either induce or inhibit senescence (Kang and Elledge, 2016; Kwon et al., 2017). Several researchers have suggested that autophagy (as a process for recycling damaged cell components) might downregulate senescence in order to prevent disorders and maintain cellular homeostasis (Hara et al., 2006; Komatsu et al., 2006). Nevertheless, autophagy might also promote senescence during infection in order to enable long-term survival, even though some cells are damaged in the process (Deruy et al., 2010; Gosselin et al., 2009; Young and Narita, 2010). Autophagy also contributes to the establishment of senescence by facilitating the release of SASP cytokines, as we observed in CM (Narita et al., 2011; Young and Narita, 2010; Young et al., 2009; Young et al., 2011). Furthermore, greater expression of P38MAPK (interacting with NF-κB, which is essential for the induction of SASP) was observed in the brain during ECM. Involvement of P38MAPK in the production of SASP via NF-κB was confirmed in senescent human astrocytes treated with a P38MAPK inhibitor; the cells secreted significantly lower amounts of SASP components (Freund et al., 2011).

Several cytokine/chemokine components of the SASP (such as IL-6, CCL-2 and CXCL-10) are significantly associated with CM (Dalko et al., 2016; Dunst et al., 2017; Shrivastava et al., 2017). Our transcriptomic data identified *Pml*, *p21*, *Calr* and *Cxcl-10* as predictors of premature senescence associated with inflammation in the brains of CM^S mice. The elevated secretion of CXCL-10, CCL-2 and TNF-α observed in *Pb*A-stimulated primary astrocyte cultures is directly dependent on the autophagy of *Pb*A-MVs (Leleu et al., 2021). It is noteworthy that the long-term maintenance of CXCL-10 production by astrocytes might depend on the senescence process, since the latter is altered or suppressed when autophagy is inhibited. This suggests causal relationships between autophagy, astrocyte senescence, and the neuroinflammatory response. Indeed, the link between astrocyte senescence and CM was confirmed in CM^R mice (which do not express the hallmarks of senescence in the brain after *Pb*A infection) and in CM^S mice protected from CM by treatment with the senolytic drugs DQ. These observations were reinforced by our modelling studies in which the CXCL-10 produced by astrocytes in response to *Pb*A-infection was a key early factor in the neuroinflammation contributing to CM. Astrocyte end-feet encircling endothelial cells have an important role in maintaining the BBB integrity (Zhang et al., 2019a,b). In CM, activated astrocytes retract their processes and distribute themselves unevenly in the vessel. Thus, senescent astrocytes characterized by the expression of p21 might impair the function of brain vessels by contributing to the loss of endothelium integrity and the increase of BBB permeability during the onset of CM.

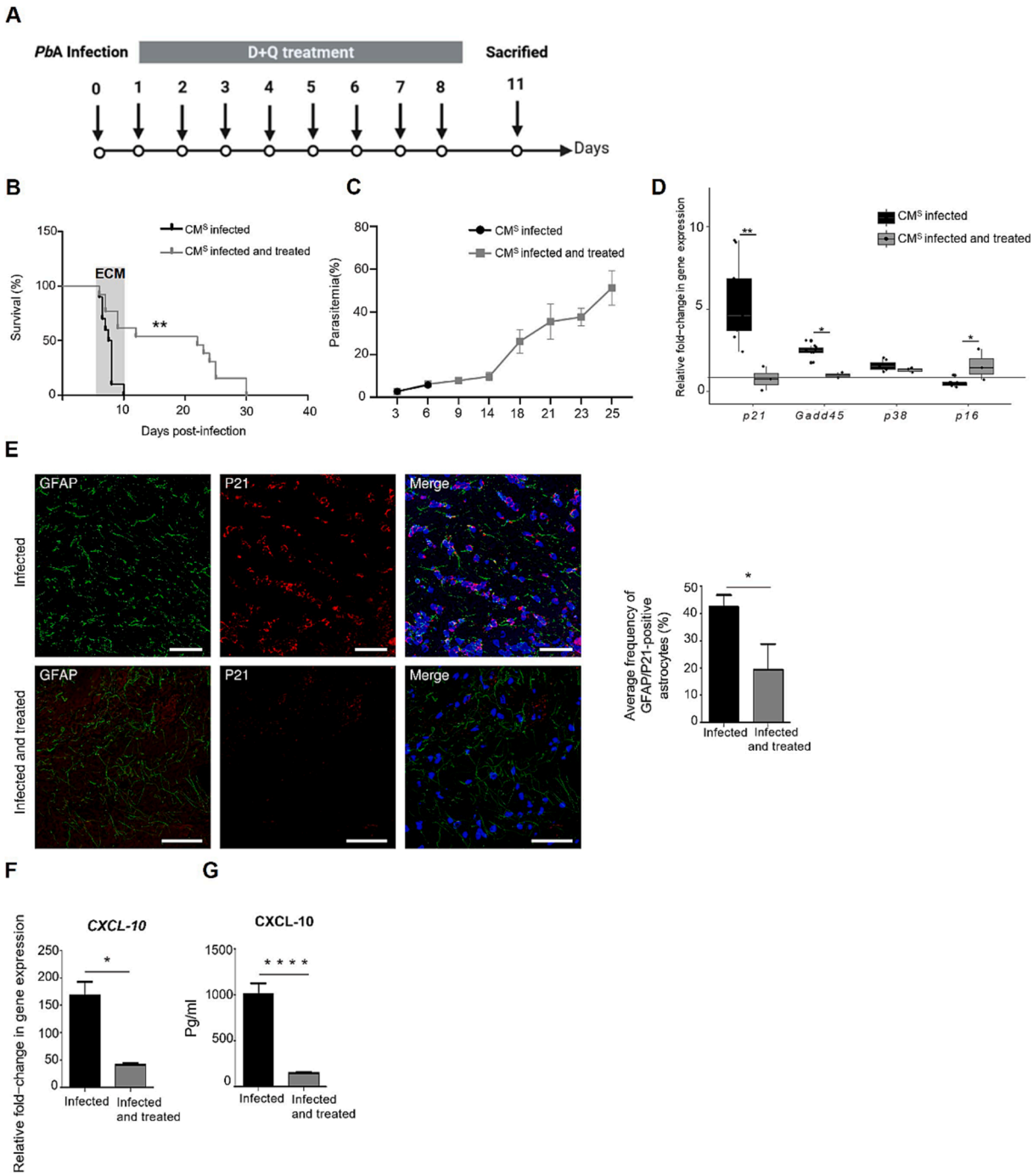

Fig. 8. Dasatinib plus Quercetin prevented ECM by eliminating senescent astrocytes. (**A**) Experimental scheme of DQ treatment (**B**) Survival and (**C**) Parasitemia rate of mice infected with *Pb*A and treated with DQ. Data are results from n = 10–13 mice that were compared using a Mantel-Cox test (**B**) or a Mann–Whitney test (**C**). (**D**) Expression of *p21*, *GADD45γ*, *p38MAPK* and *p16* genes in brain at day 6.5 post-infection for *Pb*A group and day 11 post-infection for infected and treated group. (**E**) Representative immunofluorescence images showing p21 protein levels (red) in GFAP^{+} astrocytes (green) in the brain of infected compared with infected treated mice, scale bar: 400 μm. Graphs show quantification of the percentage of GFAP/P21 positive astrocytes. (**F**) Expression levels of *CXCL-10* in the brain (n = 3–16 per group). (g) CXCL-10 protein levels in the plasma (n = 5 per group). Data are mean fold-change ± SEM. Values in c-f were compared with the infected group using Mann–Whitney test; *P < 0.05; **P < 0.01; ***P < 0.001; ****P < 0.0001.

Moreover, senescent aastrocytes by their secretome may increase the production of CCL2, CCL5, CXCL9, and CXCL10 that can exacerbate the disease by recruiting leukocytes in the brain and reduce neuronal survival during CM (Strangward P etal., 2017).

We also observed senescence on brain sections from adult CM patients, and iRBCs were sequestered in the regions that displayed GFAP^{+}p21^{+} senescent astrocytes. Senescence was also highlighted by elevated *p21* expression and low *p16* expression in PBMCs from CM and CM-MOD patients, while elevated *p16* expression was observed in MM patients.

Senescence has been already described in *P. falciparum* patients with MM; it was characterized by elevated p16 expression and telomere shortening in PBMCs (Asghar et al., 2016; Asghar et al., 2018; Miglar et al., 2021). Of note, these observation are done in adult. Major differences are known between CM in children and adults (Plewes et al., 2018). Adult CM, particularly in India, is associated with a high

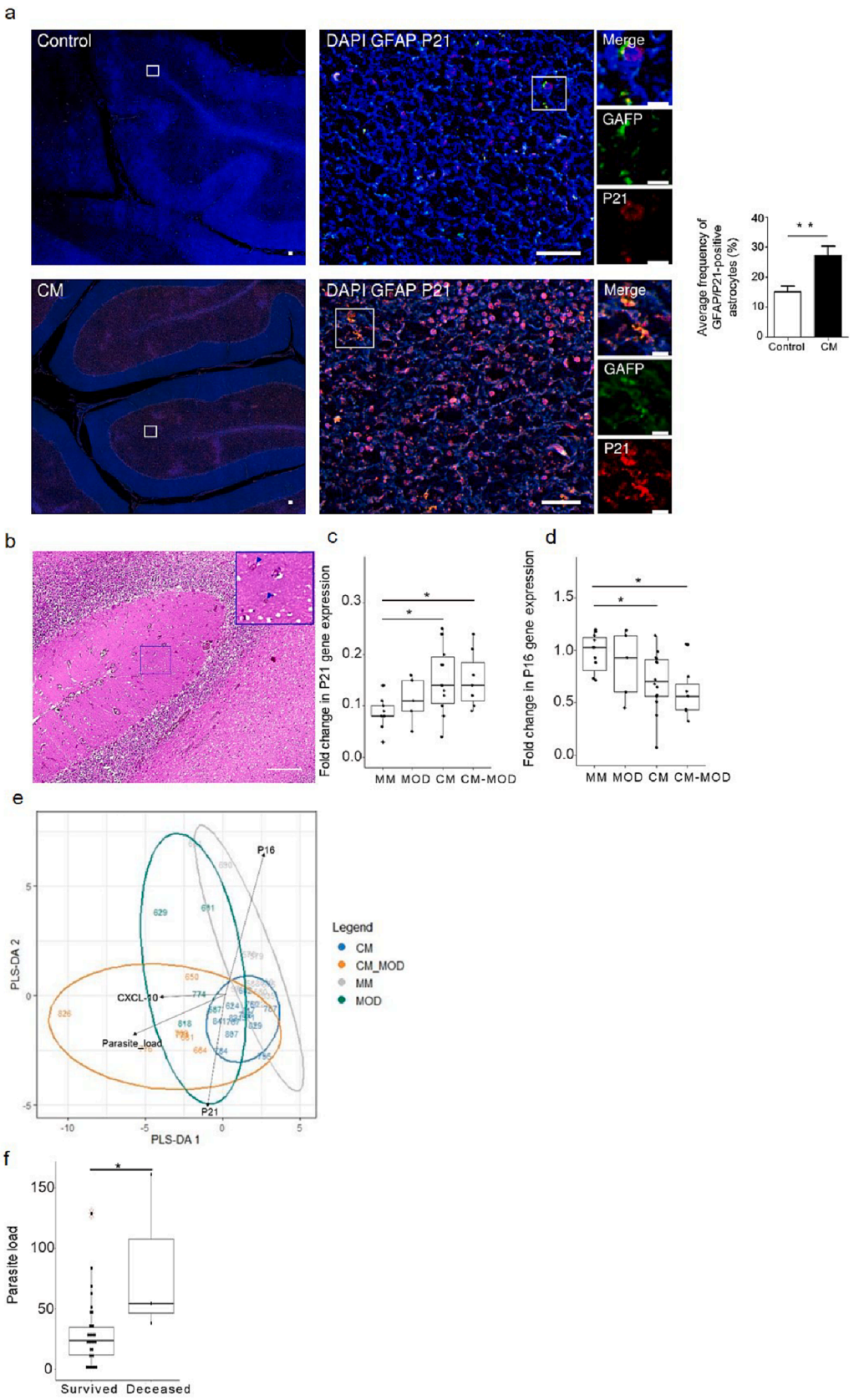

(caption on next page)

Fig. 9. p21 is expressed in peripheral blood and in brain of CM patients. (**A**) Representative images of double immunofluorescence for GFAP (green) and p21 (red) in the human brain sections of CM patients compared with controls. Patients were compared with controls using Student's *t*-test; **P < 0.01. Data are presented as median ± SEM. (**B**) Hematoxylin and eosin-stained sections of CM patient brains. Scale bar represents 100 μm. Quantification by RT-qPCR of relative (**C**) p21 and (**D**) p16 genes expression in in total PBMCs from patients from India with mild malaria (MM), isolated CM, multi-organ failure (MOD) and (CM-MOD); *P < 0.05. Groups were compared with a Kruskal-Wallis test followed by the Conover post-hoc test when significant comparing the severe cases to the mild form. Pvalues are adjusted by FDR Benjamini-Hochberg. Error bars show the median ± SEM. (**E**) Discriminant analysis showing the contribution of senescence markers, cytokines and chemokines and parasite load in different patients' groups. (**F**) Distribution of parasitic load in survived and deceased patients. Statistics data are related in Table S5.

proportion of a renal failure, whereas children may present with a more isolated CNS phenotype with more frequent ring haemorrhages and inflammatory cell accumulation in the brain microvasculature. Maturational changes in the cerebral vasculature in children may account for some of the differences in disease presentation and outcome between children and adults including long term neurological sequelae observed in children surviving CM (Sahu et al., 2021).

Our results strongly suggest that the p16/p21 balance not only has a role in astrocyte senescence in CM but is also associated with disease severity in human malaria; indeed, we found that p21-driven senescence occurred concomitantly in PBMCs and brain cells from patients with CM. Furthermore, CM-MOD (the most severe form of malaria) was associated with the highest CXCL-10 levels, elevated p21 expression, and elevated parasitaemia – particularly in patients who died. These observations further suggest that an elevated plasma CXCL-10 level and p21 expression in PBMCs are potentially valuable biomarkers for lethal malaria. These biomarkers could be assayed relatively easily in a peripheral blood sample, as has already described for Alzheimer's disease markers (Tan et al., 2012).

In conclusion, we identified a novel mechanism by which the malaria parasite can also promote an inflammatory response in the brain via a senescence pathway induced by LC3-dependent autophagy. This senescence contributes to the onset of CM and so senolytic drugs such as DQ along with artemisinin-based combination might be an adjunctive therapy for CM prevention. Lastly, the p21/CXCL-10 combination might be a biomarker of the severity and lethality of CM in humans.

Author contributions

SP, CA, BD, FT: Study concept an design. FH, IL, NS: Performed the experiments. CL: statistical analysis. DK, HYE, BD, FT, NM: Contributed to reagents/materials/analysis tools. FH, IL, NS, EW, CL: acquisition and interpretation of data. FH, IL, NS, CA, FT and SP: contribute to writing of the manuscript.

CRediT authorship contribution statement

Fatima Hellani: Formal analysis, Investigation, Methodology, Visualization, Writing – original draft. **Inès Leleu:** Formal analysis, Investigation, Resources, Validation, Writing – original draft. **Nasreddine Saidi:** Formal analysis, Investigation, Methodology, Software, Writing – original draft. **Nathalie Martin:** Resources, Validation. **Cécile Lecoeur:** Formal analysis, Methodology, Visualization, Writing – review & editing. **Elisabeth Werkmeister:** Methodology, Resources, Software. **David Koffi:** Resources, Validation. **François Trottein:** Resources. **Hélène Yapo-Etté:** Resources, Validation. **Bidyut Das:** Resources, Validation, Writing – review & editing. **Corinne Abbadie:** Conceptualization, Formal analysis, Methodology, Supervision, Validation, Writing – review & editing. **Sylviane Pied:** Conceptualization, Supervision, Validation, Writing – original draft, Writing – review & editing.

Declaration of competing interest

The authors declare that they have no known competing financial interests or personal relationships that could have appeared to influence the work reported in this paper.

Data availability

Data will be made available on request.

Acknowledgments

The authors acknowledge use of the PLETHA platform of Pasteur Institute of Lille for assistance in animal care and maintenance and are thankful to Dr. Corine Glineur (CIIL, Université de Lille, CNRS UMR 9017, Inserm U1019) for her help in siRNA experiments and for comments during the writing of the manuscript; Dr. Hélène Bauderlique (BIcell Platform) for technical assistance in flow cytometry and cell sorting. We also thank Prof Pierre-André Cazenave (CIIL, Institut Pasteur and Sorbonne University) for critical evaluation of the manuscript and Mr David Fraser, Biotech communication for content editing.

This work was supported by the LabEx PARAFRAP: ANR-11-LABX-0024 for IL and NS salaries. FH was recipient of a doctoral fellowship from Mairie de Chmestar and LabEx PARAFRAP.

Appendix A. Supplementary data

Supplementary data to this article can be found online at https://doi.org/10.1016/j.bbi.2023.12.030.

References

Abbadie, C., Pluquet, O., Pourtier, A., 2017. Epithelial cell senescence: an adaptive response to pre-carcinogenic stresses? Cell. Mol. Life Sci. 74, 4471–4509.
Asghar, M., Hasselquist, D., Hansson, B., Zehtindjiev, P., Westerdahl, H., Bensch, S., 2015. Hidden costs of infection: chronic malaria accelerates telomere degradation and senescence in wild birds. Sci. 347, 436–438.
Asghar, M., Palinauskas, V., Zaghdoudi-Allan, N., Valkiūnas, G., Mukhin, A., Platonova, E., Färnert, A., Bensch, S., Hasselquist, D., 2016. Parallel telomere shortening in multiple body tissues owing to malaria infection. *Proceedings of the Royal Society of London b: Biological Sciences* 283:20161184.
Asghar, M., Yman, V., Homann, M.V., Sonden, K., Hammar, U., Hasselquist, D., Farnert, A., 2018. Cellular aging dynamics after acute malaria infection: A 12-month longitudinal study. Aging Cell 17, e12702.
Baker, D.J., Petersen, R.C., 2018. Cellular senescence in brain aging and neurodegenerative diseases: evidence and perspectives. J. Clin. Invest. 128, 1208–1216.
Baptista, F.G., Pamplona, A., Pena, A.C., Mota, M.M., Pied, S., Vigario, A.M., 2010. Accumulation of Plasmodium berghei-infected red blood cells in the brain is crucial for the development of cerebral malaria in mice. Infect. Immun. 78, 4033–4039.
Benarroch, E.E., 2013. Microglia Multiple roles in surveillance, circuit shaping, and response to injury. Neurol. 81, 1079–1088.
Birch, J., Gil, J., 2020. Senescence and the SASP: many therapeutic avenues. Genes Dev. 34, 1565–1576.
Boivin, M.J., Bangirana, P., Byarugaba, J., Opoka, R.O., Idro, R., Jurek, A.M., John, C.C., 2007. Cognitive impairment after cerebral malaria in children: a prospective study. Pediatrics 119, e360–e366.
Carter, J.A., Mung'ala-Odera, V., Neville, B.G., Murira, G., Mturi, N., Musumba, C., Newton, C.R., 2005. Persistent neurocognitive impairments associated with severe falciparum malaria in Kenyan children. J. Neurol. Neurosurg. Psychiatry 76, 476–481.
Childs, B.G., Baker, D.J., Kirkland, J.L., Campisi, J., Van Deursen, J.M., 2014. Senescence and apoptosis: dueling or complementary cell fates? EMBO Rep. 15, 1139–1153.
Childs, B.G., Gluscevic, M., Baker, D.J., Laberge, R.M., Marquess, D., Dananberg, J., van Deursen, J.M., 2017. Senescent cells: an emerging target for diseases of ageing. Nat. Rev. Drug Discov. 16, 718–735.
Choi, J.-Y., Park, J.H., Jo, C., Kim, K.-C., Koh, Y.H., 2022. SARS-CoV-2 spike S1 subunit protein-mediated increase of beta-secretase 1 (BACE1) impairs human brain vessel cells. Biochem. Biophys. Res. Commun. 626, 66–71.
Cohen, J., Torres, C., 2019. Astrocyte senescence: Evidence and significance. Aging Cell 18, e12937.
Coppe, J.P., Desprez, P.Y., Krtolica, A., Campisi, J., 2010. The senescence-associated secretory phenotype: the dark side of tumor suppression. Annu. Rev. Pathol. 5, 99–118.

Dalko, E., Genete, D., Auger, F., Dovergne, C., Lambert, C., Herbert, F., Cazenave, P.A., Roland, J., Pied, S., 2016. Heme dampens T-cell sequestration by modulating glial cell responses during rodent cerebral malaria. Brain Behav. Immun. 58, 280–290.
Debacq-Chainiaux, F., Erusalimsky, J.D., Campisi, J., Toussaint, O., 2009. Protocols to detect senescence-associated beta-galactosidase (SA-betagal) activity, a biomarker of senescent cells in culture and in vivo. Nat. Protoc. 4, 1798–1806.
Deruy, E., Gosselin, K., Vercamer, C., Martien, S., Bouali, F., Slomianny, C., Bertout, J., Bernard, D., Pourtier, A., Abbadie, C., 2010. MnSOD upregulation induces autophagic programmed cell death in senescent keratinocytes. PLoS One 5, e12712.
Dominique, M., Josiane, N., Marianna, I.-B., 2000. Cerebral malaria and immunogenetics. Parasite Immunol. 22, 613–623.
Dunst, J., Kamena, F., Matuschewski, K., 2017. Cytokines and chemokines in cerebral malaria pathogenesis. Front. Cell. Infect. Microbiol. 7, 324.
Freund, A., Patil, C.K., Campisi, J., 2011. p38MAPK is a novel DNA damage response-independent regulator of the senescence-associated secretory phenotype. EMBO J. 30, 1536–1548.
Gosselin, K., Deruy, E., Martien, S., Vercamer, C., Bouali, F., Dujardin, T., Slomianny, C., Houel-Renault, L., Chelli, F., De Launoit, Y., Abbadie, C., 2009. Senescent keratinocytes die by autophagic programmed cell death. Am. J. Pathol. 174, 423–435.
Hara, T., Nakamura, K., Matsui, M., Yamamoto, A., Nakahara, Y., Suzuki-Migishima, R., Yokoyama, M., Mishima, K., Saito, I., Okano, H., Mizushima, N., 2006. Suppression of basal autophagy in neural cells causes neurodegenerative disease in mice. Nature 441, 885–889.
Haupt, Y., Maya, R., Kazaz, A., Oren, M., 1997. Mdm2 promotes the rapid degradation of p53. Nature 387, 296–299.
Herbert, F., Tchitchek, N., Bansal, D., Jacques, J., Pathak, S., Becavin, C., Fesel, C., Dalko, E., Cazenave, P.A., Preda, C., Ravindran, B., Sharma, S., Das, B., Pied, S., 2015. Evidence of IL-17, IP-10, and IL-10 involvement in multiple-organ dysfunction and IL-17 pathway in acute renal failure associated to Plasmodium falciparum malaria. J. Transl. Med. 13, 369.
Hernandez-Segura, A., Nehme, J., Demaria, M., 2018. Hallmarks of cellular senescence. Trends Cell Biol. 28, 436–453.
Herranz, N., Gil, J., 2018. Mechanisms and functions of cellular senescence. J. Clin. Invest. 128, 1238–1246.
Idda, M.L., W.G. McClusky, V. Lodde, R. Munk, K. Abdelmohsen, M. Rossi, and M. Gorospe. Survey of senescent cell markers with age in human tissues. *Aging (Albany NY)* 12:4052-4066.
Idro, R., Jenkins, N.E.N., C.r.j. c., 2005. Pathogenesis, clinical features, and neurological outcome of cerebral malaria. The Lancet Neurology 4, 827–840.
Jain, V., Armah, H.B., Tongren, J.E., Ned, R.M., Wilson, N.O., Crawford, S., Joel, P.K., Singh, M.P., Nagpal, A.C., Dash, A.P., Udhayakumar, V., Singh, N., Stiles, J.K., 2008. Plasma IP-10, apoptotic and angiogenic factors associated with fatal cerebral malaria in India. Malar. J. 19, 83–86.
Kang, C., Elledge, S.J., 2016. How autophagy both activates and inhibits cellular senescence. Autophagy 12, 898–899.
Keswani, T., Roland, J., Herbert, F., Delcroix-Genete, D., Bauderlique-Le Roy, H., Gaayeb, L., Cazenave, P.A., Pied, S., 2020. Expression of CD300lf by microglia contributes to resistance to cerebral malaria by impeding the neuroinflammation. Genes Immun. 21, 45–62.
Khakh, B.S., Sofroniew, M.V., 2015. Diversity of astrocyte functions and phenotypes in neural circuits. Nat. Neurosci. 18, 942–952.
Komatsu, M., Waguri, S., Chiba, T., Murata, S., Iwata, J., Tanida, I., Ueno, T., Koike, M., Uchiyama, Y., Kominami, E., Tanaka, K., 2006. Loss of autophagy in the central nervous system causes neurodegeneration in mice. Nature 441, 880–884.
Kossod, S.D., Grau, G.E., 1993. Role of Cytokines and Adhesion Molecules in Malaria Immunopathology. Stem Cells 11, 41–48.
Kwon, Y., Kim, J.W., Jeoung, J.A., Kim, M.S., Kang, C., 2017. Autophagy Is Pro-Senescence When Seen in Close-Up, but Anti-Senescence in Long-Shot. Mol. Cells 40, 607–612.
Leleu, I., Genete, D., Desnoulez, S.S., Saidi, N., Brodin, P., Lafont, F., Tomavo, S., Pied, S., 2021. A noncanonical autophagy is involved in the transfer of Plasmodium-microvesicles to astrocytes. Autophagy 18, 1583–1598.
Lozano-Gerona, J., Garcia-Otin, A.L., 2018. ImageJ-based semiautomatic method to analyze senescence in cell culture. Anal. Biochem. 543, 30–32.
Miglar, A., Reuling, I.J., Yap, X.Z., Farnert, A., Sauerwein, R.W., Asghar, M., 2021. Biomarkers of cellular aging during a controlled human malaria infection. Sci. Rep. 11, 18733.
Minagar, A., Shapshak, P., Fujimura, R., Ownby, R., Heyes, M., Eisdorfer, C., 2002. The role of macrophage/microglia and astrocytes in the pathogenesis of three neurologic disorders: HIV-associated dementia, Alzheimer disease, and multiple sclerosis. J. Neurol. Sci. 202, 13–23.
Narita, M., Young, A.R., Arakawa, S., Samarajiwa, S.A., Nakashima, T., Yoshida, S., Hong, S., Berry, L.S., Reichelt, S., Ferreira, M., Tavare, S., Inoki, K., Shimizu, S., Narita, M., 2011. Spatial coupling of mTOR and autophagy augments secretory phenotypes. Science 332, 966–970.
Plewes, K., Turner, G.D.H., Dondorp, A.M., 2018. Pathophysiology, clinical presentation, and treatment of coma and acute kidney injury complicating falciparum malaria. *Curr Opin Infect Dis*. 31, 69–77.
Pluquet, O., Pourtier, A., Abbadie, C., 2015. The unfolded protein response and cellular senescence. A review in the theme: cellular mechanisms of endoplasmic reticulum stress signaling in health and disease. Am. J. Physiol. Cell Physiol. 308, C415–C425.
Rayess, H., Wang, M.B., Srivatsan, E.S., 2012. Cellular senescence and tumor suppressor gene p16. Int. J. Cancer 130, 1715–1725.
Rufini, A., Tucci, P., Celardo, I., Melino, G., 2013. Senescence and aging: the critical roles of p53. Oncogene 32, 5129–5143.
Sahu, P.K., Duffy, F.J., Dankwa, S., Vishnyakova, M., Majhi, M., Pirpamer, L., Vigdorovich, V., Bage, J., Maharana, S., Mandala, W., Rogerson, S.J., Seydel, K.B., Taylor, T.E., Kim, K., Sather, D.N., Mohanty, A., Mohanty, R.R., Mohanty, A., Pattnaik, R., Aitchison, J.D., Hoffmann, A., Mohanty, S., Smith, J.D., Bernabeu, M., Wassmer, S.C., 2021. Determinants of brain swelling in pediatric and adult cerebral malaria. JCI Insight. 22, e145823.
Shan-Rong, S., Marc, E.K., Krishan, L.K., 1991. Antigen retrieval in formalin-fixed, paraffin-embedded tissues: an enhancement method for immunohistochemical staining based on microwave oven heating of tissue sections. J. Histochem. Cytochem. 39, 741–748.
Shaw, T.N., Stewart-Hutchinson, P.J., Strangward, P., Dandamudi, D.B., Coles, J.A., Villegas-Mendez, A., Gallego-Delgado, J., van Rooijen, N., Zindy, E., Rodriguez, A., Brewer, J.M., Couper, K.N., Dustin, M.L., 2015. Perivascular Arrest of CD8+ T cells is a signature of experimental cerebral malaria. PLoS Pathog. 11, e1005210.
Shrivastava, S.K., Dalko, E., Delcroix-Genete, D., Herbert, F., Cazenave, P.A., Pied, S., 2017. Uptake of parasite-derived vesicles by astrocytes and microglial phagocytosis of infected erythrocytes may drive neuroinflammation in cerebral malaria. Glia 65, 75–92.
Strangward, P., Haley, M.J., Shaw, T.N., Schwartz, J.M., Greig, R., Mironov, A., de Souza, J.B., Cruickshank, S.M., Craig, A.G., Milner Jr, D.A., Allan, S.M., Couper, K. N., 2017. A quantitative brain map of experimental cerebral malaria pathology. PLoS Pathog. 13, e1006267.
Tan, M., Wang, S., Song, J., Jia, J., 2012. Combination of p53(ser15) and p21/p21 (thr145) in peripheral blood lymphocytes as potential Alzheimer's disease biomarkers. Neurosci. Lett. 516, 226–231.
Tominaga, T., Shimada, R., Okada, Y., Kawamata, T., Kibayashi, K., 2019. Senescence-associated-beta-galactosidase staining following traumatic brain injury in the mouse cerebrum. PLoS One 14, e0213673.
Vazquez-Villasenor, I., Garwood, C.J., Heath, P.R., Simpson, J.E., Ince, P.G., Wharton, S. B., 2020. Expression of p16 and p21 in the frontal association cortex of ALS/MND brains suggests neuronal cell cycle dysregulation and astrocyte senescence in early stages of the disease. Neuropathol. Appl. Neurobiol. 46, 171–185.
Wang, J., Liu, Y., Xia, Q., Xia, Q., Wang, B., Yang, C., Liang, J., Liu, X., 2020. Potential roles of telomeres and telomerase in neurodegenerative diseases. Int. J. Biol. Macromol. 163, 1060–1078.
2021. World Health Organization.
Yosef, R., Pilpel, N., Tokarsky-Amiel, R., Biran, A., Ovadya, Y., Cohen, S., Vadai, E., Dassa, L., Shahar, E., Condiotti, R., 2016. Directed elimination of senescent cells by inhibition of BCL-W and BCL-XL. Nat. Commun. 7, 1–11.
Young, A.R., Narita, M., 2010. Connecting autophagy to senescence in pathophysiology. Curr. Opin. Cell Biol. 22, 234–240.
Young, A.R., Narita, M., Ferreira, M., Kirschner, K., Sadaie, M., Darot, J.F., Tavare, S., Arakawa, S., Shimizu, S., Watt, F.M., Narita, M., 2009. Autophagy mediates the mitotic senescence transition. Genes Dev. 23, 798–803.
Young, A.R., Narita, M., Narita, M., 2011. Spatio-temporal association between mTOR and autophagy during cellular senescence. Autophagy 7, 1387–1388.
Zhang, Z., et al., 2019b. The appropriate marker for astrocytes: comparing the distribution and expression of three astrocytic markers in different mouse cerebral regions. Biomed Res. Int. 24, 9605265.
Zhang, P., Kishimoto, Y., Grammatikakis, l., Gottimukkala, K., Cutler, R.G., Zhang, S., Abdelmohsen, K., Bohr, V.A., Sen, J.M., Gorospe, M., Mattson, M.P., 2019a. Senolytic therapy alleviates Abeta-associated oligodendrocyte progenitor cell senescence and cognitive deficits in an Alzheimer's disease model. Nat. Neurosci. 22, 719–728.